# REPORT DOCUMENTATION PAGE

AFRL-SR-BL-TR-01-

*0023*

| 1. AGENCY USE ONLY *(Leave blank)* | 2. REPORT DATE | 3. |  |
|---|---|---|---|
|  | 31 Oct 00 | Final Tech Report | 1 Mar 96 to 28 Feb 98 |

**4. TITLE AND SUBTITLE**
Theoretical and Numerical Validation of Scalar EM Propagation Modeling Using
Parabolic Equations and the Pade Rational Operator Approximation

**5. FUNDING NUMBERS**
F49620-96-1-0060

**6. AUTHOR(S)**
Dr. Ronald Brent

**7. PERFORMING ORGANIZATION NAME(S) AND ADDRESS(ES)**
Department of Mathematical Sciences
University of Massachusetts Lowell
Lowell, MA 01854

**8. PERFORMING ORGANIZATION
REPORT NUMBER**

**9. SPONSORING/MONITORING AGENCY NAME(S) AND ADDRESS(ES)**
Air Force Office of Scientific Research
AFOSR/NM
801 N. Randolph Street, Rm 732
Arlington, VA 22203-1977

**10. SPONSORING/MONITORING
AGENCY REPORT NUMBER**

F49620-96-1-0060

**11. SUPPLEMENTARY NOTES**

**12a. DISTRIBUTION AVAILABILITY STATEMENT**
Approved for public release; distribution unlimited.

**12b. DISTRIBUTION CODE**

**13. ABSTRACT** *(Maximum 200 words)*

The problem associated with the absorbing layers had been addressed and solved. The code has been benchmarked against analytical solutions and shown to be accurate to within .01 dB. The enclosed figures show excellent agreement between the computed and exact solution over a variety of frequencies. While the transmission loss for an infinite medium is frequency independent, which is why all the solutions are identical, the construct of the absorbing layer is frequency dependent. This is why I checked a variety of input frequencies between 1 MHz and 50 MHz. The following pages contain output showing exact(analytical) solutions and 2 numerical solutions, one with the absorbing layer and one without. One can clearly see that the absorbing layer correctly dampens any energy associated with reflections from nonphysical (finite numerical domain) boundaries.

Unfortunately it took most of the contract period to do so, hence none of the original objectives were accomplished.

Also appended to this report is an updated user manual containing user information, as well as an interpolation and source sensitivity analysis.

DTIC QUALITY INSPECTED 4

**20010124 137**

**14. SUBJECT TERMS**

**15. NUMBER OF PAGES**

**16. PRICE CODE**

| 17. SECURITY CLASSIFICATION OF REPORT | 18. SECURITY CLASSIFICATION OF THIS PAGE | 19. SECURITY CLASSIFICATION OF ABSTRACT | 20. LIMITATION OF ABSTRACT |
|---|---|---|---|
| UNCLASSIFIED | UNCLASSIFIED | UNCLASSIFIED | UL |

Theoretical and numerical validation of scalar EM propagation modeling using parabolic equations and the Pade rational operator approximation.
F49620-96-1-0060

Final Report

Dr. Ronald Brent
Department of Mathematical Sciences
University of Massachusetts Lowell
Lowell MA 01854
(978) 934-2440 (Phone)
(978) 934-3053 (Fax)
Ronald_Brent@uml.edu (email after 6/1/2000)

## ORIGINAL OBJECTIVES

*   Benchmarking the numerical techniques used including a sensitivity analysis.
*   Developing and enhancing the numerical code by:
    *   Studying how to interpolate the refraction profiles on the field mesh.
    *   Implementing a finite element algorithm.
    *   Incorporating troposcatter and sky wave propagation

## INTERMEDIATE OBJECTIVES

*   Build a working absorbing layer below the Earth's surface.
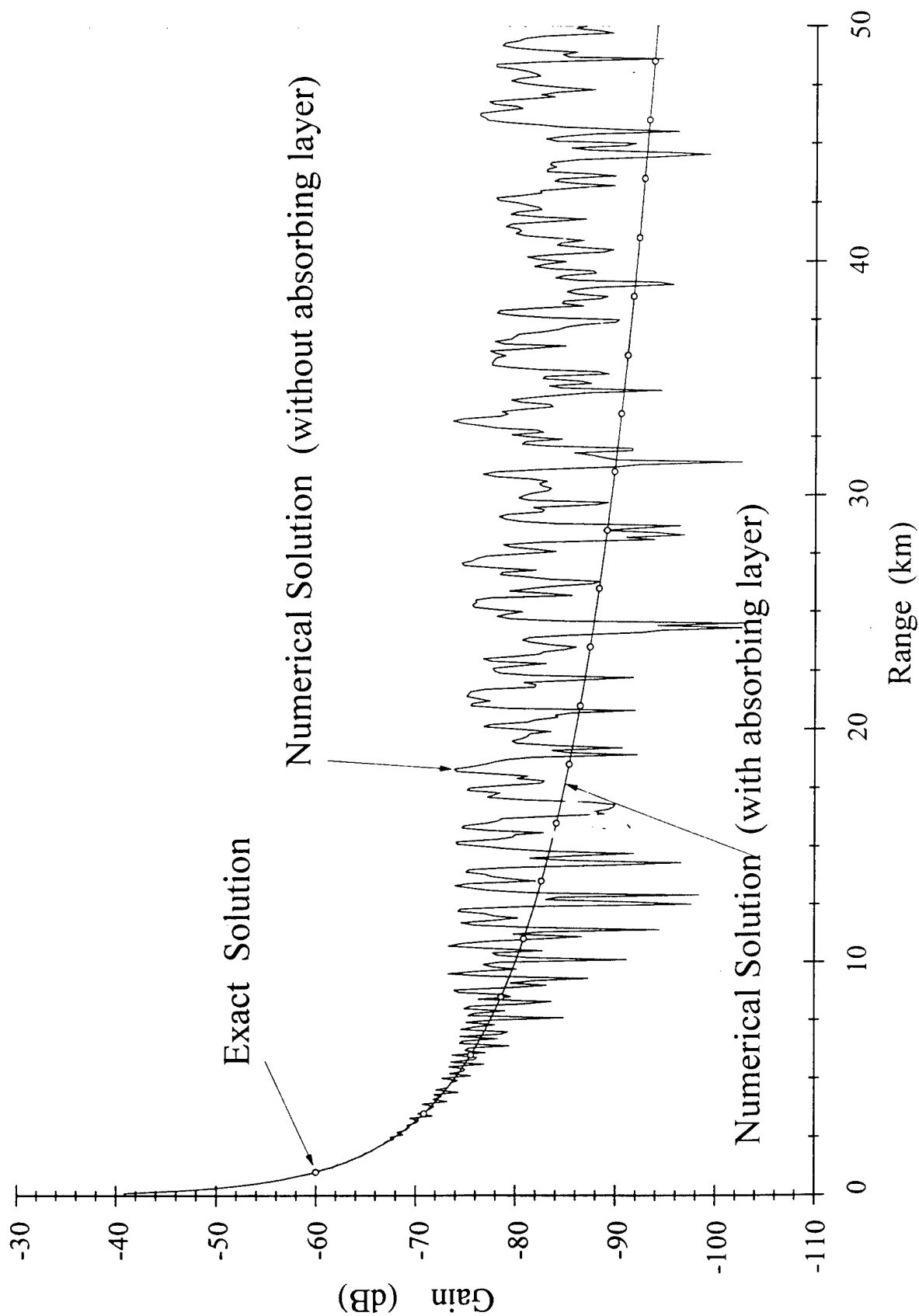*   Benchmark the layer against simple analytical models

## FINAL STATUS

The problem associated with the absorbing layers had been addressed and solved. The code has been benchmarked against analytical solutions and shown to be accurate to within .01 dB. The enclosed figures show excellent agreement between the computed and exact solution over a variety of frequencies. While the transmission loss for an infinite medium is frequency independent, which is why all the solutions are identical, the construct of the absorbing layer is frequency dependent. This is why I checked a variety of input frequencies between 1 MHz and 50 MHz. The following pages contain output showing exact(analytical) solutions and 2 numerical solutions, one with the absorbing layer and one without. One can clearly see that the absorbing layer correctly dampens any energy associated with reflections from nonphysical (finite numerical domain) boundaries.

Unfortunately it took most of the contract period to do so, hence none of the original objectives were accomplished.

Also appended to this report is an updated user manual containing user information, as well as an interpolation and source sensitivity analysis.

Absorbing Layer Comparison (f=1MHz, hmax1=3000=-hmax2) wf=15

Exact Solution

Numerical Solution (without absorbing layer)

Numerical Solution (with absorbing layer)

Gain (dB)

Range (km)

Absorbing Layer Comparison (f=5MHz, hmax1=-hmax2=3000)  wf=2

Exact Solution

Numerical Solution  (without absorbing layers)

Numerical Solution  (with absorbing layers)

Range (km)

Gain (dB)
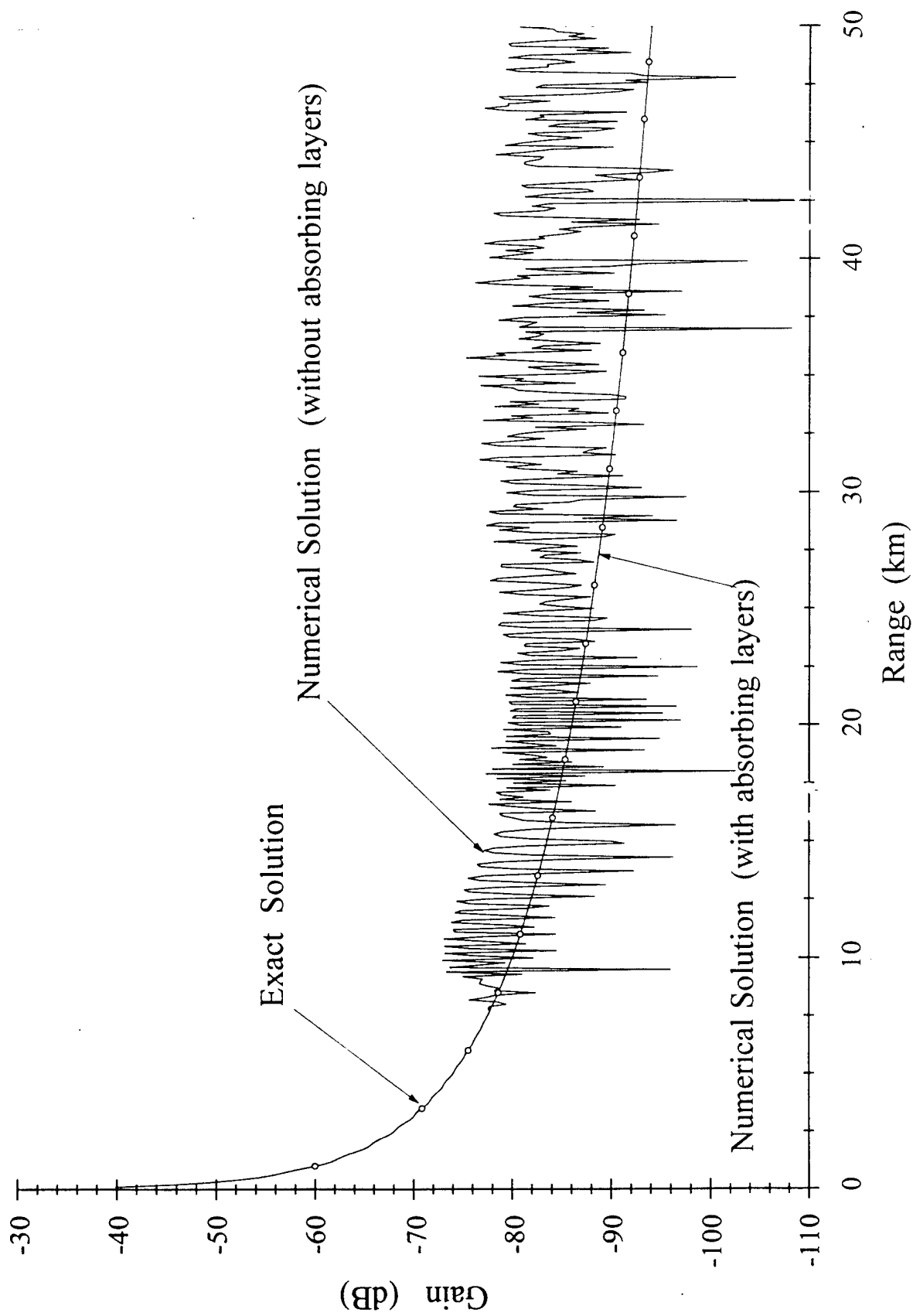
Absorbing Layer Comparison (f=10MHz, hmax1=-hmax2=3000)  wf=1

Exact Solution

Numerical Solution  (without absorbing layers)

Numerical Solution  (with absorbing layers)

Range (km)

Gain (dB)
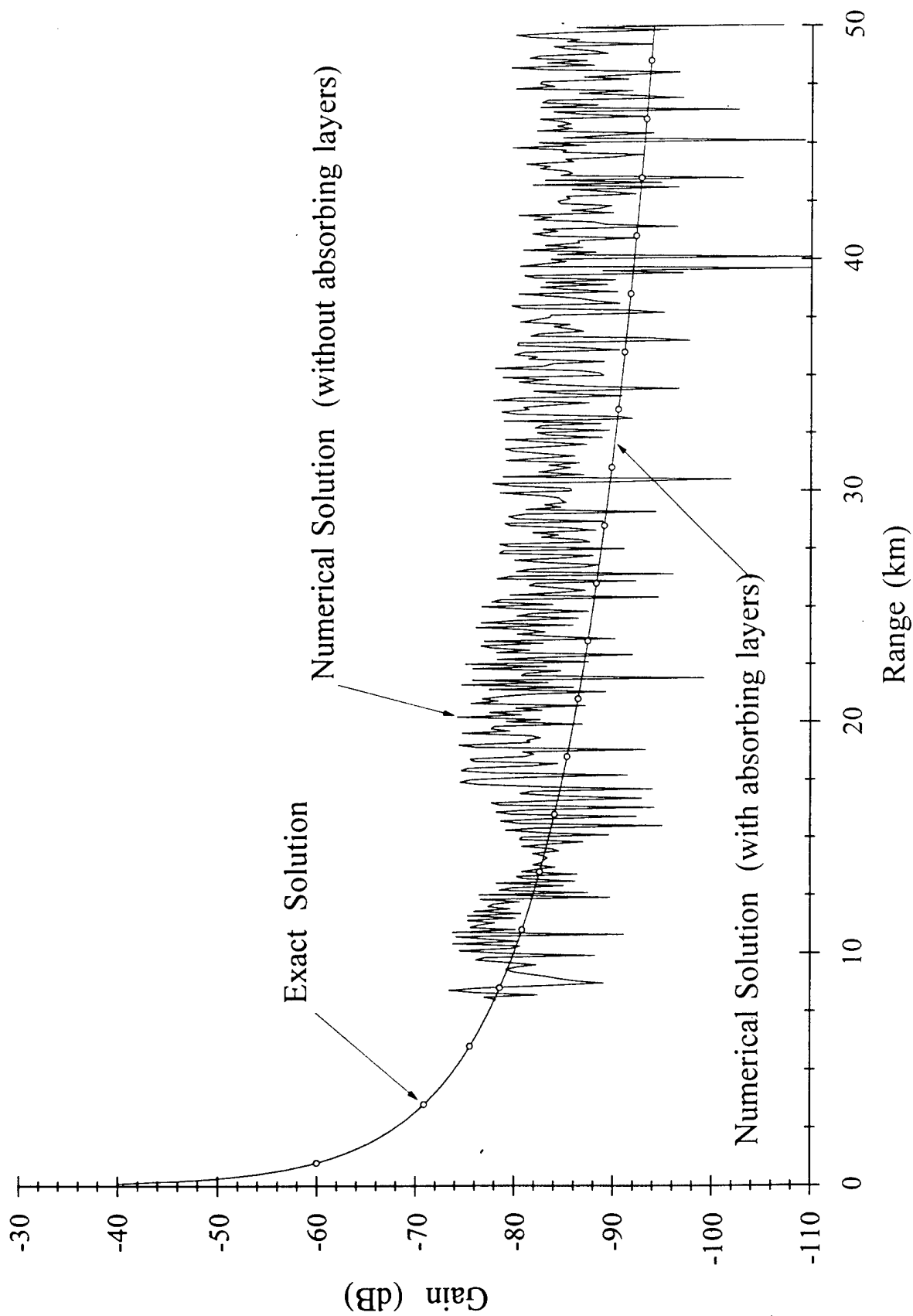
Absorbing Layer Comparison (f=20MHz, hmax1=3000=-hmax2)   wf=1/3
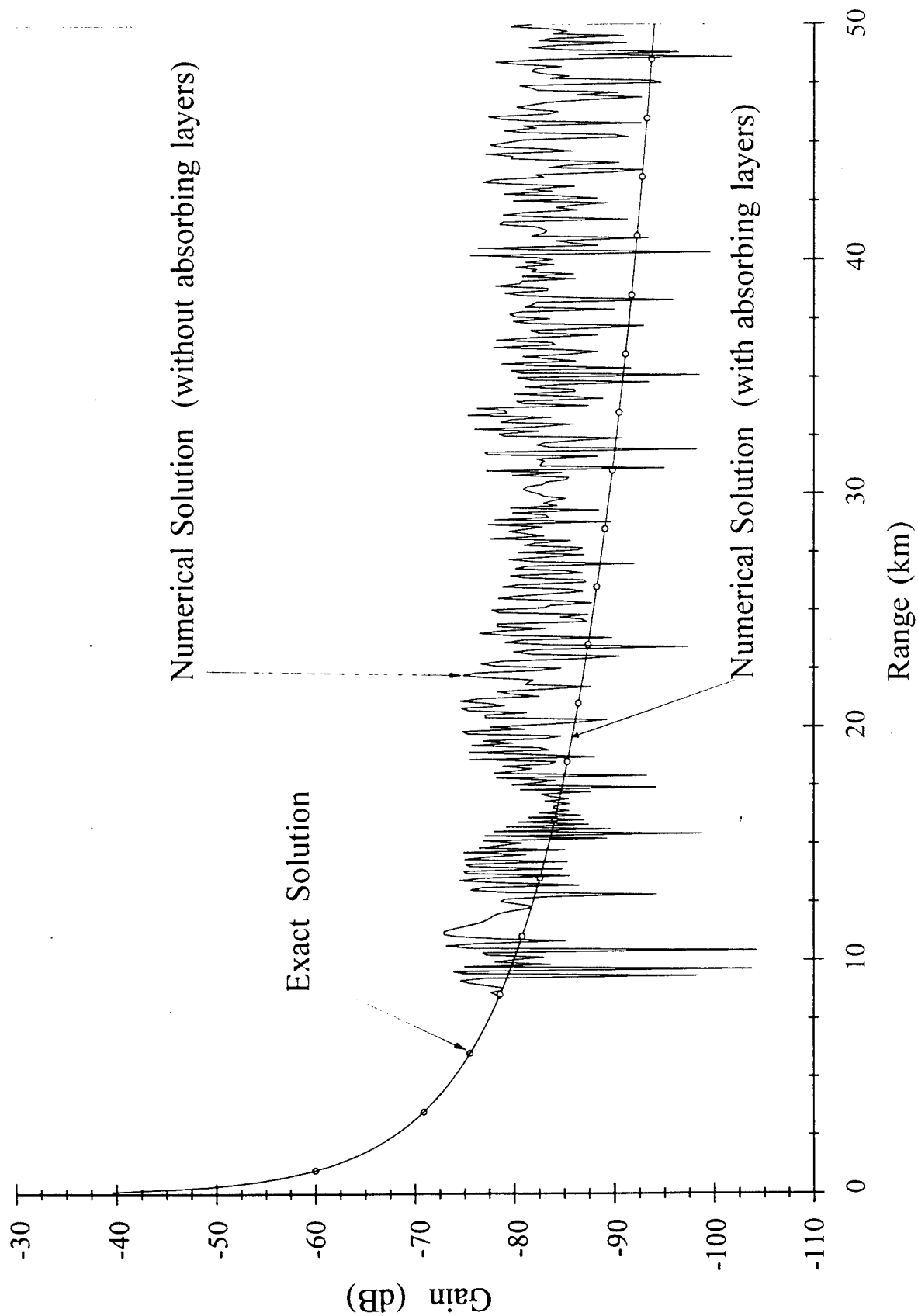
Absorbing Layer Comparison (f=25MHz, hmax1=3000=-hmax2)  wf=1/3
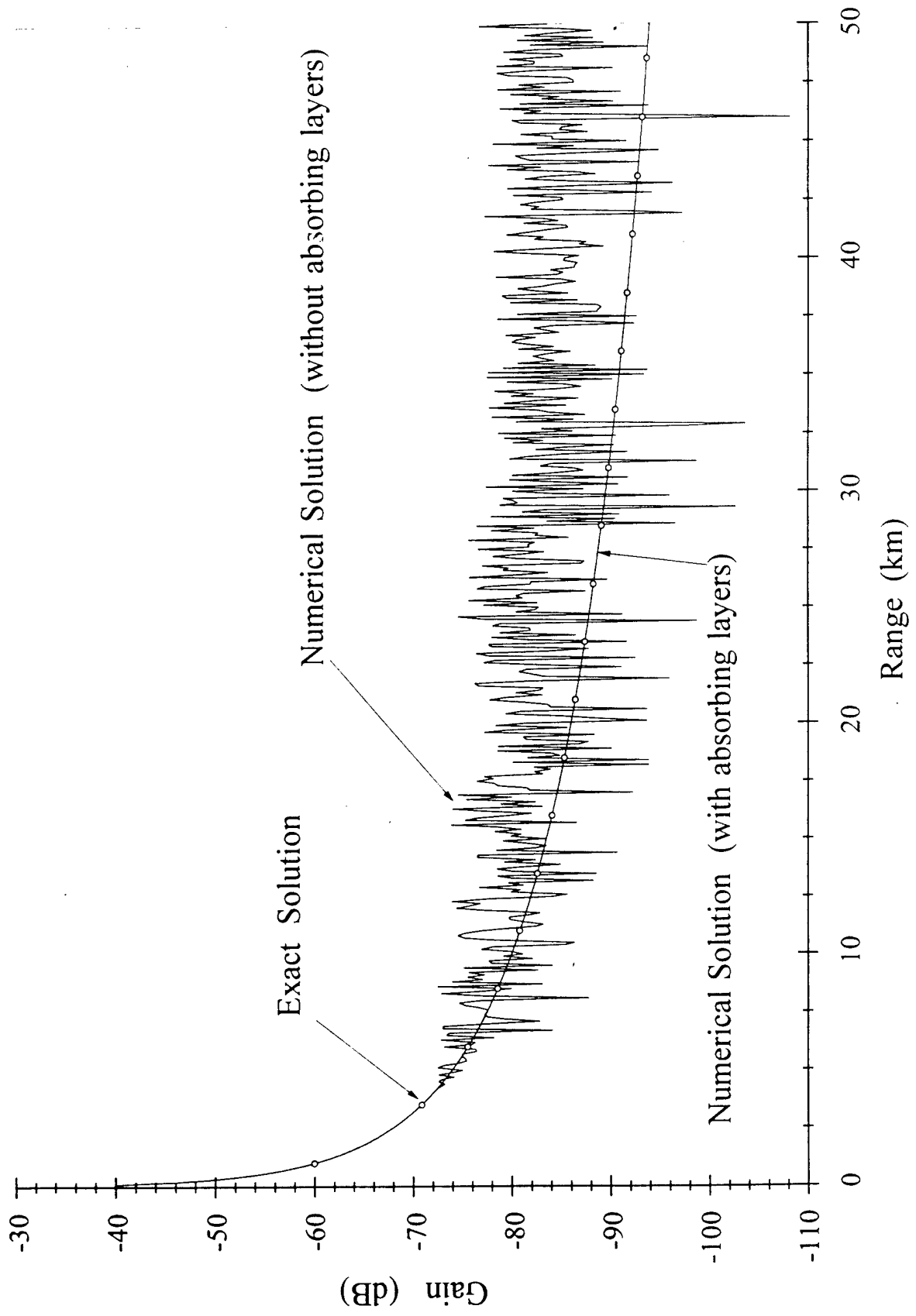
Absorbing Layer Comparison (f=50MHz hmax1=3000=-hmax2) wf=1/3
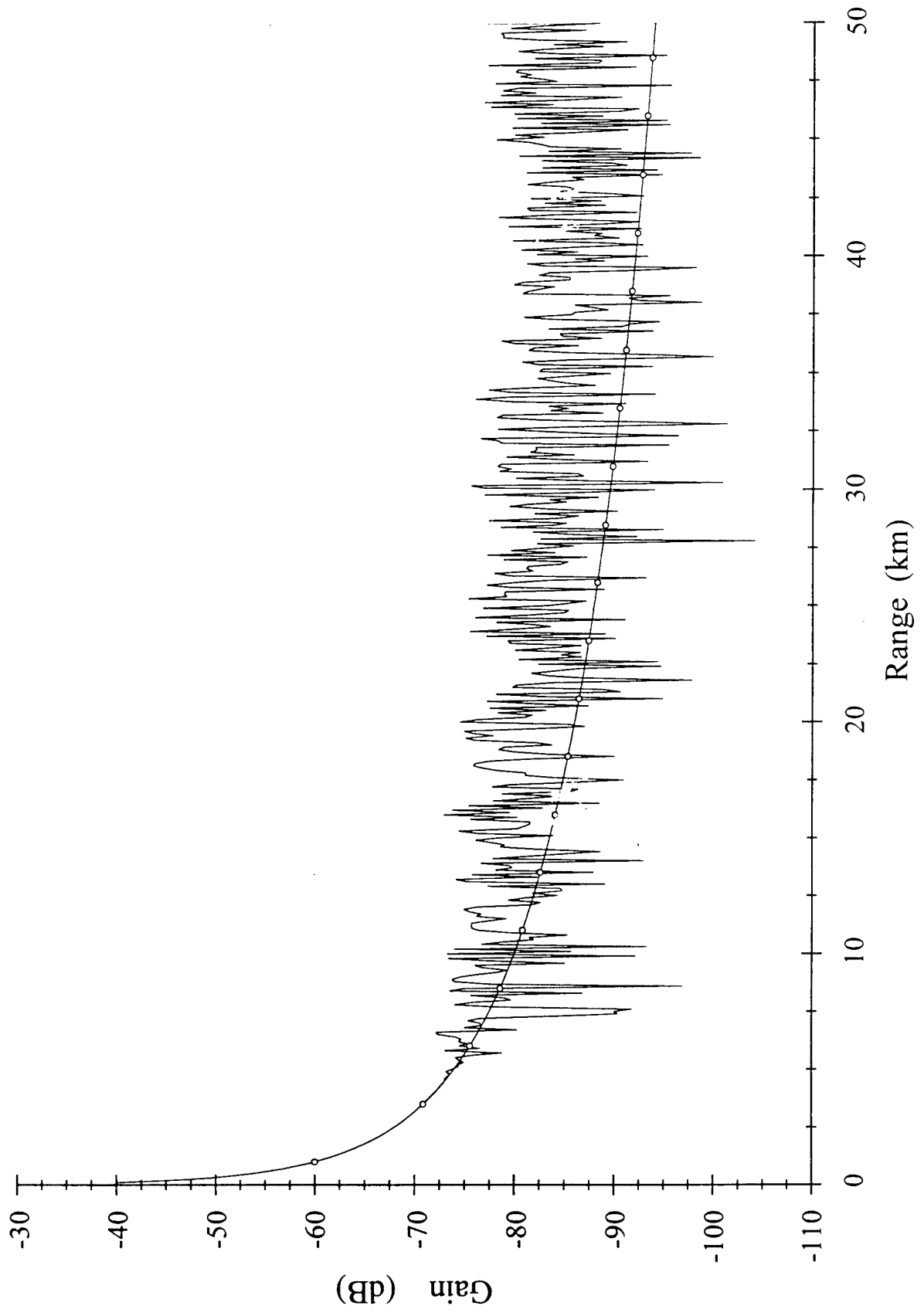
# SSP:User Manual

by

**Dr. Ronald Brent**
**Department of Mathematical Sciences**
**University of Massachusetts Lowell**
**Lowell MA 01854**
**(978) 934-2440 (Phone)**
**(978) 934-3053 (Fax)**
**Ronald_Brent@uml.edu**

# Abstract

This report contains updated user information for the program **SSP**. This program is an implementation of the Pade series approximation for parabolic equations modeling one-way scalar 2-D electromagnetic propagation. The code can be run on PC's with Pentium processors. The current program is set for 20,000 notch points in height and NPADE $\leq 8$. The code is written in generic FORTRAN and has been compiled using Microsoft-FORTRAN Powerstation. The accompanying CD contains source and executable codes for **SSP** as well as **EPADE**, the code responsible for calculating the Pade coefficients. Also on the CD is a graphics program **GRAPH1** and **SSPPREP** an input file preparation program dsigned to make setting up input files more user friendly. **GRAPH** is a screen graphic contour programs for displaying results immediately. This program is written in *C* and source codes are also included.

# I. Program Description

Under certain simplifying assumptions one may reduce the solution of the full 3-D vector electromagnetic propagation problem to that of two simpler scalar models. These problems correspond to horizontally or vertically polarized wave fields. A full discussion of the analysis and derivations leading to such equations is given in References 1 and 2. The primary assumption leading to this reduction or splitting of the vector problem into scalar pieces is medium symmetry in at least one coordinate direction. The reader is referred to Ref. 1 before reading this report. We will assume that the user is familiar with that report and the notations and descriptions contained therein. The program SSP is the numerical implementation of the results of that report. It is a finite difference approach for solving parabolic equations modeling scalar EM propagation.

The program SSP consists of a main routine which calls a total of 13 other subroutines or functions. The subroutine hierarchy is illustrated in Figure 1. Subroutine Descriptions are as follows:

**INPUT**        This subroutine is responsible for reading in all input parameters other than field profiles. This input resides in the first 7 lines of the file SSP.IN, and the next n lines determining the terrain elevation. If the user requests an absorbing layer, INPUT calls the subroutine SPONGE, and uses the function CRVCORR.

**CRVCORR**   This function is used in implementing the curvature correction when using the Earth-Flattening transformation.

**PROFL**       Responsible for input of all profile data which resides in the lines following the topography input. PROFL calls the subroutine READQ.

**READQ**       Responsible for reading in medium profiles and interpolating the profiles over the entire height grid.

**CC**             Responsible for computing the width of the artificial absorbing layer at the top of the atmosphere. For a given frequency, using tabular data, absorbing layer widths are interpolated and passed back to INPUT.

**GREEN**    Creates a Green's function starting field. It uses the function
$$FGS(ARG) = \exp(-ARG/4)$$

**MODES**    Creates a Homogeneous Normal Mode Starting Field. This is a nice startup field because at allows limitation of the aperture using THMAX.

**GAUSS**    Creates the typical Gaussian Starting field. It uses the function
$$FGR(ARG) = (1.4467 - 0.4201*ARG)*\exp(-ARG/3.0512)$$

**MATRC**    This subroutine sets up the matrices used in solving the linear system associated with the Pade discretization of the Parabolic Equation.

**UPDAT**    This subroutine is used to update the matrices whenever there is a change in the bottom topography.

**SOLVE**    This subroutine solves the tridiagonal system of equations associated with the discretization. This subroutine is called every time a step in range is taken.

The program flow is quite simple. For a given medium, the basic flow is a loop in range in which the solution of a tridiagonal matrix problem is calculated. After each step, receiver loss values are interpolated and then written to a file. The matrices involved in the linear system are composed of tridiagonal entries dependent upon grid width, $dz$, medium parameters, such as refraction and conductivity, as well as interface coupling. Each time any one of these parameters changes the matrices must be re-computed. The two subroutines MATRC and UPDAT are responsible for setting up these matrices. The subroutine MATRC is used whenever there is a new set of profiles in the input run-stream. For terrain elevation changes UPDAT is used. The subroutines UPDAT and MATRC do exactly the same thing however when there is only a change in terrain elevation, and not refraction, one need only re-compute the matrix elements for a small sub-set of equations in the entire linear system. The program runs far more efficiently using UPDAT. Running the code using MATRC alone is possible, and in fact is a good check if adapting this code in that area.

A general flow of the program is given in Figure 2. This is only a rough outline of the code to give the reader a feel for the program.
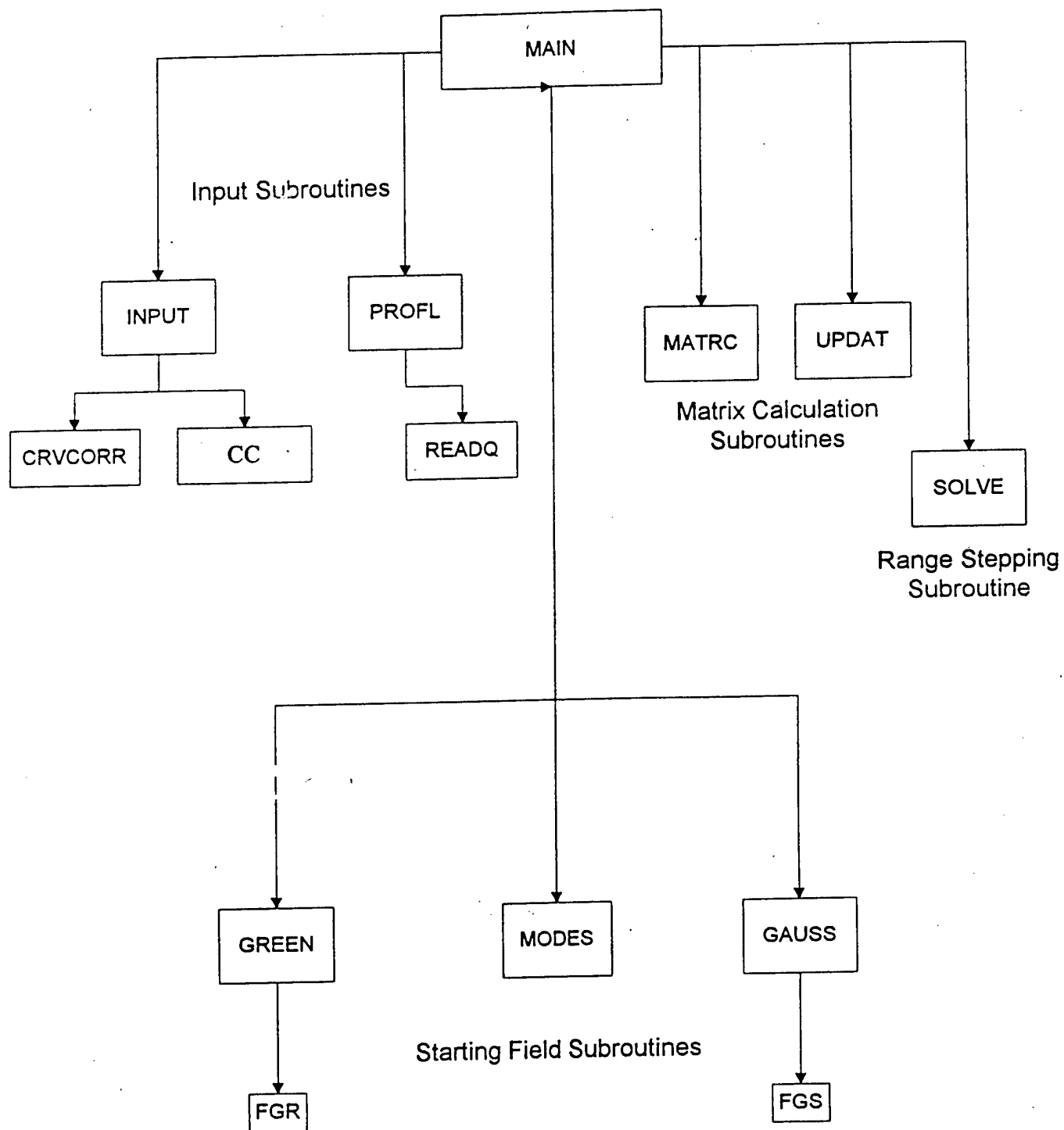
# SSP PROGRAM STRUCTURE



Figure 1
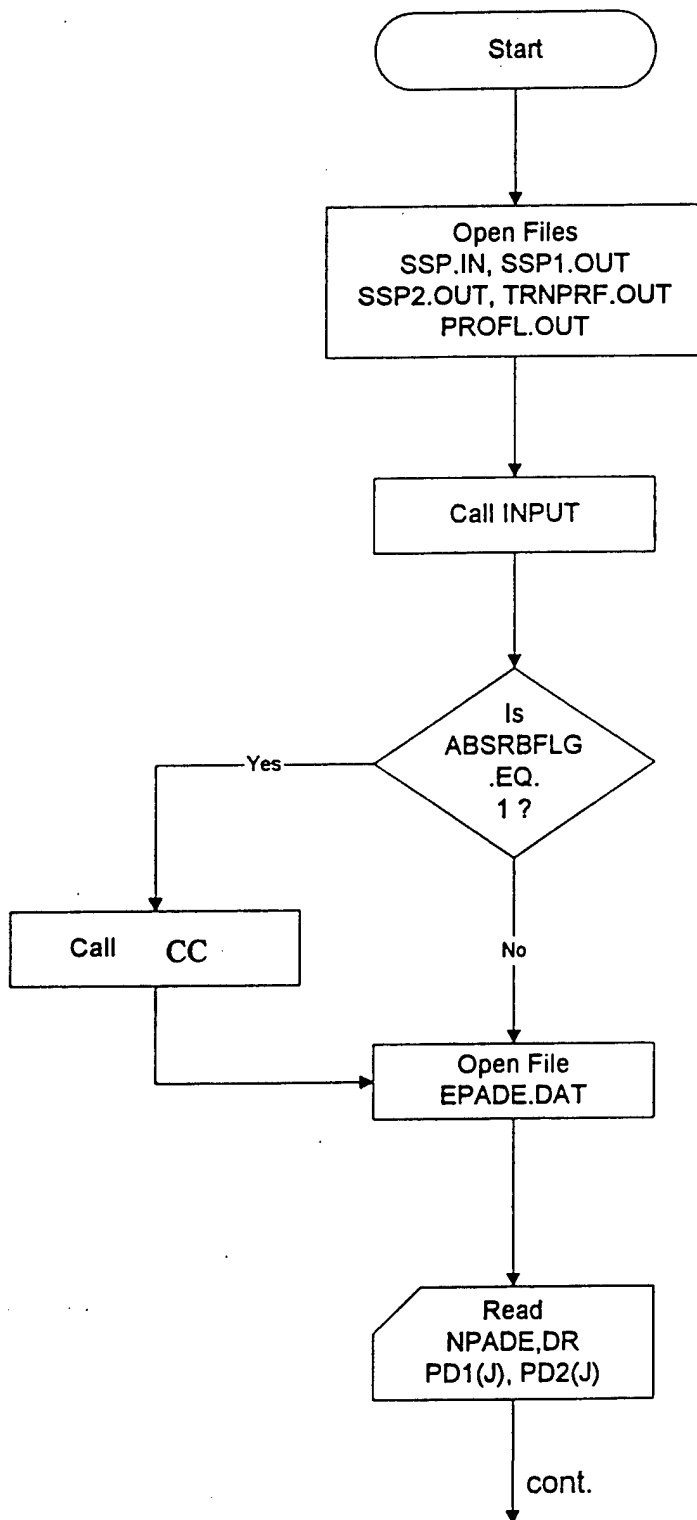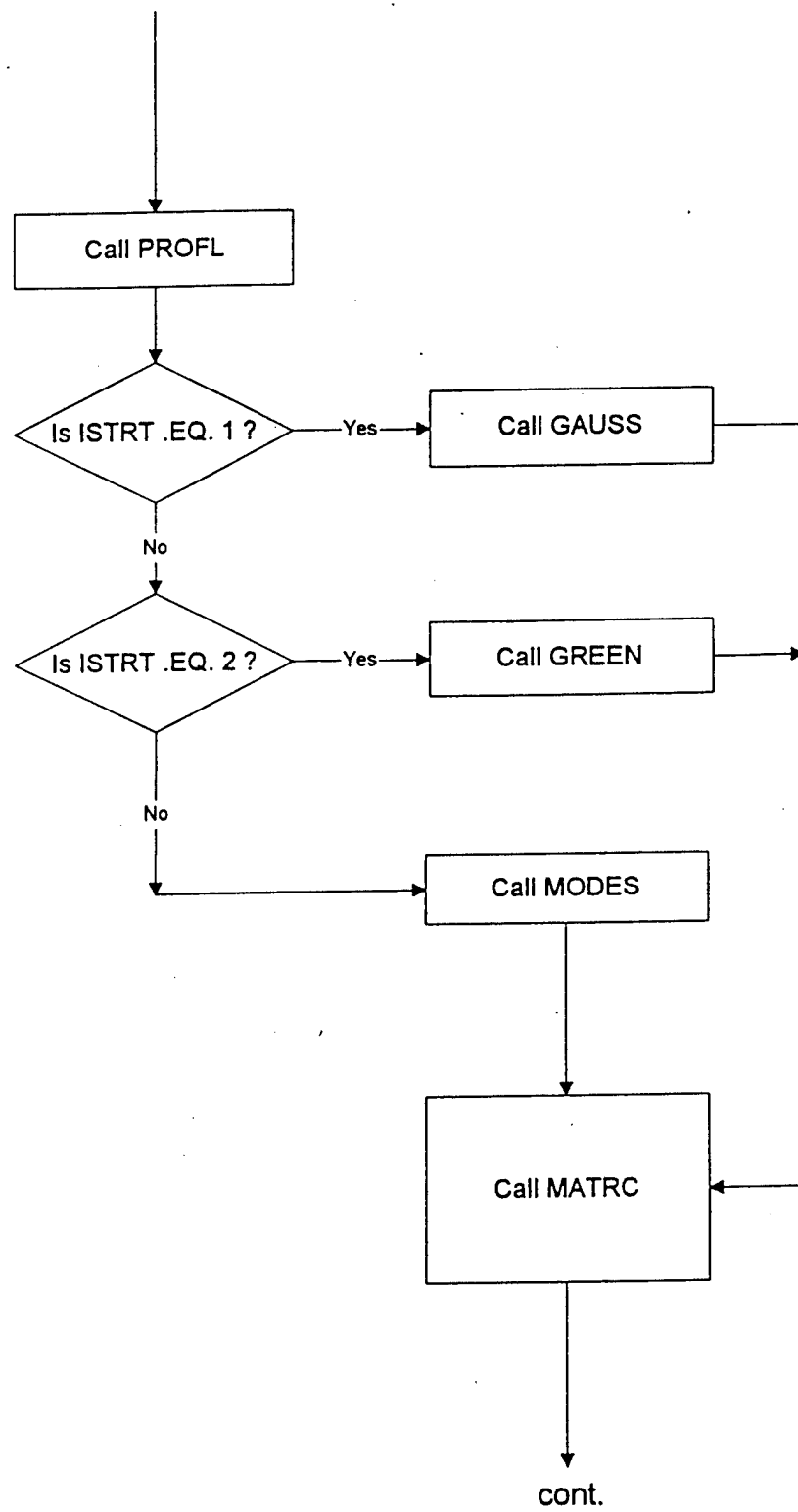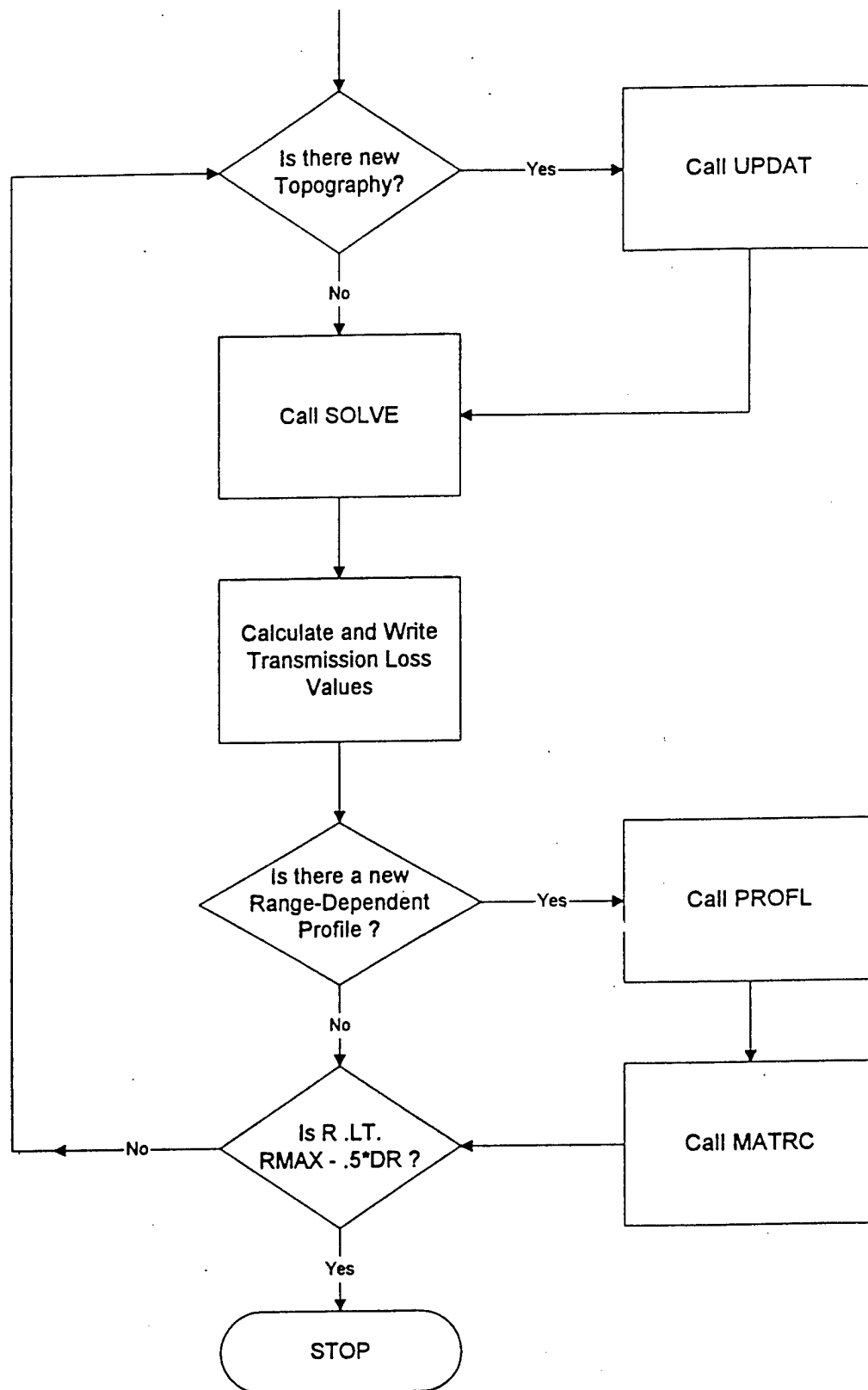
5

# SSP Flow Chart



Figure 2

Figure 2 cont.

Figure 2 cont.

## II. Input Run-Stream

The input for the program comes from two files. The first file EPADE.DAT must be produced by using the program **EPADE**. This program automatically reads physical information from the primary input file, SSP.IN, and produces EPADE.DAT containing the Pade coefficients. The input file SSP.IN is where the user specifies all the information pertaining to source and receiver configurations as well as the medium topography and refraction profiles. The disk containing the source and executable codes also has a directory with some sample input files. It is recommended that a user first become familiar with those files and modify them for their own use.

The input in the file SSP.IN is grouped into three sections. The first section, which is contained in the first seven lines of the file, is where the source and receiver configuration is specified. Output options are also specified there along with parameters needed for the screen graphics post-processing program **GRAPH**. The next section is the terrain profile. The remaining section itself consists of sub-sections. The medium dielectric and conductive properties are entered as a series of range-independent sets of profiles. That is at specified ranges, height dependent profiles are entered. There is no interpolation in range. The medium is assumed vertically stratified until the following range with changes is reached. A complete description of the input records with associated definitions is given in the following pages. The next section contains some example input run-streams and their associated output.

# Input Run-Stream

***********
## CARD 1
***********

TITLE

TITLE:   Title for Input Data and Graphics Plot. After the Title (20 Characters) one should type the word "TITLE", i.e. in columns 21-25. This is necessary for the post-processing graphics program, **GRAPH**.

***********
## CARD 2
***********

FREQ, ZS, ZR, POLFLG, ABSRBFLG

FREQ:   Source Frequency in MHz.

ZS:   Source Height (above MSL) in meters.

ZR:   Receiver Height (above MSL) in meters.

POLFLG:   Polarization Flag ( POLFLG=0 for Horizontal Polarization POLFLG=1 for Vertical Polarization )

ABSRBFLG:   Atmospheric Absorbing layer Flag ( ABSRBFLG=1 will extend the atmosphere by the amount WIDTH as computed by the subroutine CC.)

***********
## CARD 3
***********

RMAX, DR, NDR

RMAX:   Maximum Range for Calculations in kilometers.

DR:   Computational range step in meters.

NDR:   Number of notch point skips in range in writing entire field.

\*\*\*\*\*\*\*\*\*\*\*

## CARD 4

\*\*\*\*\*\*\*\*\*\*\*

HMAX1, HMAX2, DZ, NDZ, ZTPLT, ZBPLT

| | |
|---|---|
| HMAX1: | Maximum height of Atmosphere in meters. |
| HMAX2: | Maximum Depth of Terrain in meters. |
| DZ: | Computational height step in meters. |
| NDZ: | Number of notch point skips in height in writing entire field. |
| ZTPLT: | Used for contour plot. Top of the graph in meters |
| ZBPLT: | Used for contour plot. Bottom of the graph in meters |

NOTE:    All heights are measured relative to MSL (z=0).HMAX2 gives the elevation of the bottom of the calculational domain. (Usually negative)

\*\*\*\*\*\*\*\*\*\*\*

## CARD 5

\*\*\*\*\*\*\*\*\*\*\*

GL(i)  i=1,13

GL(I):    These are contour level values (positive) for use by the post processing program GRAPH, which produces screen-graphic contour plots of loss values

\*\*\*\*\*\*\*\*\*\*\*

## CARD 6

\*\*\*\*\*\*\*\*\*\*\*

NPADE, (IFLAG(I),I=1,4)

NPADE:    The number of terms in the Pade approximation series.

IFLAG(1):    Write Flag for the output file PROFL.OUT. This file contains interpolated input profiles. IFLAG(1) = 1 turns the write statements on.

IFLAG(2):     Write Flag for the output file TRNPRF.OUT which contains interpolated terrain profile heights. IFLAG(2) = 1 turns the write statements on.

IFLAG(3):     Write Flag for the output file SSP1.OUT. IFLAG(3) = 1 turns the write statements on. If using the graphics program GRAPH this must be set equal to 1.

IFLAG(4):     Output option flag for artificially setting loss values = 500 dB for receiver locations below the terrain. This will make for more distinct graphics output when using the post-proccessing program GRAPH. IFLAG(4)=1 causes 500 dB substitution. If choosing this option, it is best to pick GL(13) = 499.

\*\*\*\*\*\*\*\*\*\*\*\*

## CARD 7

\*\*\*\*\*\*\*\*\*\*\*\*

ISTRT, THMAX

ISTRT:     Starting field type flag
= 1 gives a Gaussian starting field.
= 2 gives a Green's function staring field.
= 3 gives a Normal Mode starting field using a point omni-directional point source. Aperture is limited by THMAX

THMAX:     Maximum angle for mode starting field. Useful in limiting the source aperture. Used only in ISTRT=3.

**\*\*\*\*\*\*\*\*\*\*\*\*\*\***

**CARD 8+**    Terrain Elevation Data Input ( < 500 data points)

**\*\*\*\*\*\*\*\*\*\*\*\*\***

RD(1), D(1)

RD(2), D(2)

.

.

.    Range RD in kilometers and elevation D in meters.

.

.

RD(N1), D(N1)


**\*\*\*\*\*\*\*\*\*\*\*\*\*\***

**CARD 8+N1**    Atmospheric N Profile.

**\*\*\*\*\*\*\*\*\*\*\*\*\*\***

Z(1), CW(1)

Z(2), CW(2)

.    Height Z in meters.

.    Refraction CW in N-units.

.    NOTE:  Z(i) must be less than Z(i+1).

Z(N2), CW(N2)


**\*\*\*\*\*\*\*\*\*\*\*\*\*\*\*\***

**CARD 8+N1+N2**   Terrain Dielectric Input Profile.

**\*\*\*\*\*\*\*\*\*\*\*\*\*\*\*\***

Z(1), CB(1)

Z(2), CB(2)

.    Height Z in meters.

.    Relative Permittivity CB.

.    NOTE:  Z(i) < Z(i+1).

Z(N3), CB(N3)

```
*********************
```
**CARD 8+N1+N2+N3**      Terrain Conductivity Input Profile.
```
*********************
```

Z(1), COND(1)
Z(2), COND(2)
    .        Height Z in meters
    .        Conductivity COND in MHO/m
    .        NOTE: $Z(i)$ must be less than $Z(i+1)$.
Z(N4), COND(N4)

```
*************************
```
**CARD 7+N1+N2+N3+N4**
```
*************************
```

RP

    RP:   Range in kilometers of the next profile.

```
*************************
```
CARDS 7+N1+N2+N3+N4++
```
*************************
```

Repeat the previous three sections for each range profile.

Once an input file has been set up, the user then runs the program **EPADE**. This program automatically reads the input data DR, FREQ, and NPADE, from the file SSP.IN and then produces a file called EPADE.DAT which contains the complex series coefficients. This file is then read by the program **SSP**. The program **EPADE** is a modification of one written by Dr. Michael Collins. A description of the numerical methods used in that program can be found in Ref. 3. You will get a message from **EPADE** if the code does not converge. If this is the case you must either decrease the range step-size DR, or increase the number of terms in the series, NPADE.

### Program SSPREP

I have written a precursor program called **SSPPREP** which is designed to create input files for the novice user. It prompts the user for all physical information, such as source and receiver configuration, terrain elevation, and atmospheric makeup, and then creates an input file called SSP.IN in the format appropriate for the code SSP.

The code **SSPPREP** allows for terrain following refractive profiles. I put this in since there is some data available that suggests that near coastal regions, atmospheric refraction profiles may tend to slope up with the land as the terrain rises. Terrain topography can be input as *(x,y)* data pairs (typical), or as a sinusoidal model with user specified amplitude and period. Both the input files used in samples 1 and 3 were created using **SSPPREP**.

If you use **SSPPREP** the input file that is created should have parameter values that *should yield convergent solutions.* There is a possibility of the code crashing if the parameters ZTPLT and ZBPLT are not chosen correctly.

### III. Output Options

There are several output options for the code. Primary output is in the two files SSP1.OUT and SSP2.OUT. For a requested receiver height, SSP2.OUT contains the loss values at each range step between $r = 0$ and $r =$ RMAX. The file SSP1.OUT is a binary file used by the program **GRAPH**. It contains field loss values on a grid specified by the user in Card 4 through parameters ZTPLT and ZBPLT. These are the elevations of the top and bottom, respectively, of the graph. NDR and NDZ give the output steps. Currently the graphics programs accept grid sizes with the total number of range points between 250 and 1000, and the total number of height points between 125 and 500. If the user requests too many height output points the program will automatically change NDZ to accommodate the output. Range steps NDR must be correctly entered by the user however, if the graphics program is used. Choose NDR so that RMAX/(NDR*DR) is between 250 and 1000, where RMAX is measured in meters. I wished the output to this file to be as general as possible for other uses. This is why NDR and NDZ were not hard coded.

For debugging purposes, it was also nice to have the interpolated medium refraction values for the entire height array. By choosing IFLAG(1) = 1, one obtains these values in the file PROFL.OUT. Interpolated terrain elevation may also be obtained in the file TRNPRF.OUT if one chooses the option IFLAG(2) = 1. I left this option in for future graphics programs. Currently, the screen-graphics program **GRAPH** creates contour plots and by using the option IFLAG(4) = 1, all points below the terrain are given values of 500 dB losses. This way by specifying GL(13) = 499, one obtains clear graphical depiction of the ground. Future codes will show true losses and use TRNPRF.OUT to drawn in the Earth's terrain elevation.

## IV Sample Input Files

The following two tables contain samples of input files used to produce Figures 3 and 4. Table 1 gives the input file for Example 1, and Table 2 gives the input file for Example 2. The input files can be found on the program CD.

### Table 1:  Example 1 Input File

```
Lloyds Mirror                 TITLE
   4.9965   75.00   75.00 0 0     FREQ ZS  ZR POLFLG ABSRBFLG
   4.000    2.000   4            RMAX DR NDR
 100.00 -100.00  .500  1   100.00 -100.00 HMAX1 HMAX2 DZ NDZ TPLT BPLT
 30.0 35.0 40.0 45.0 50.0 55.0 60.0 65.0 70.0 75.0 80.0 85.0 90.0
  4 0 1 1 0                 NPADE (IFLAG(I),I=1,4)
 3 89.50                    ISTRT THMAX
   .0000      .0000         RD(i)  d(i)  Terrain Data Point
  -999       -999
   .0000      .0000          z(i)   N(i)
  -999       -999
   .0000     1.0000          z(i)   EPS(i)
  -999       -999
   .0000      .0000          z(i)   SIGMA(i)
  -999       -999
```
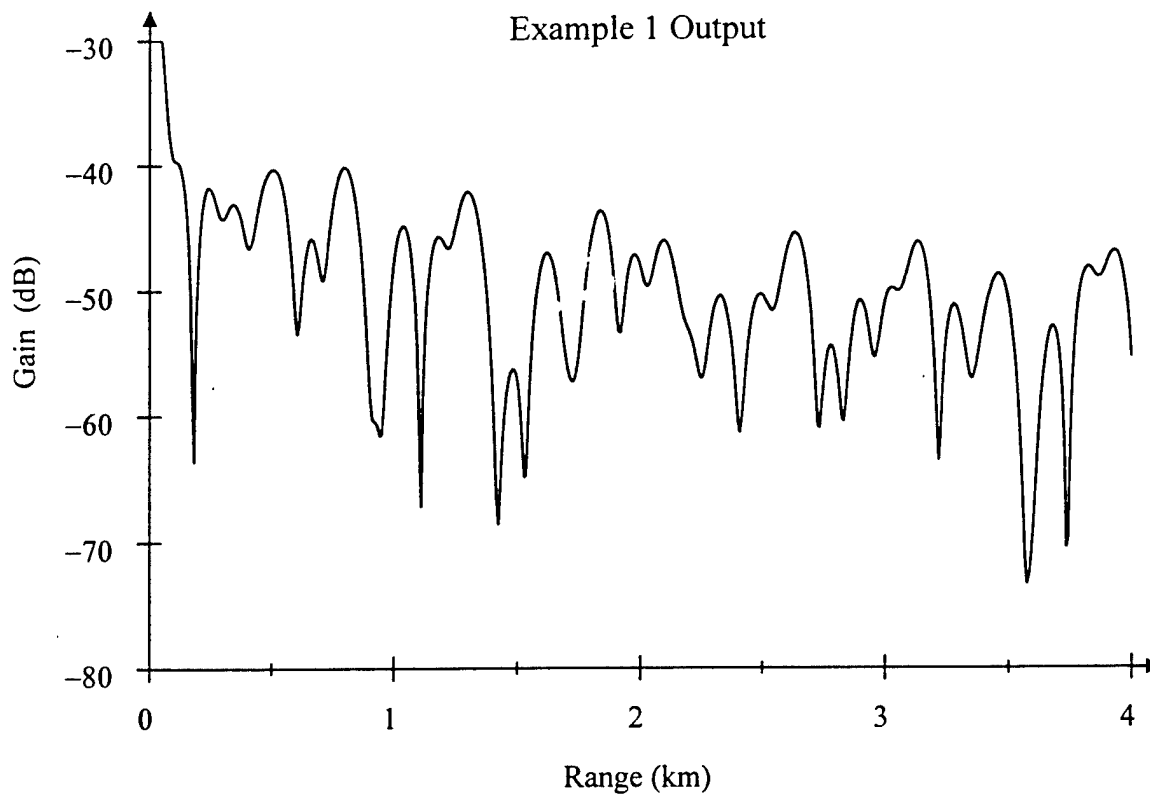


Figure 3

## Table 2: Example 2 Input File

```
Sinusoidal Terrain              TITLE
  25.0000  250.00  250.00 1 1    FREQ ZS  ZR POLFLG ABSRBFLG
  50.000    5.000    10          RMAX DR NDR
1200.00  -500.00  .999  6 1200.00 -200.00 HMAX1 HMAX2 DZ NDZ TPLT BPLT
  60.0 65.0  70.0  75.0  80.0  85.0  90.0  95.0 100.0 105.0 110.0 120.0 499.0
   4 0 0 1 1                     NPADE (IFLAG(I),I=1,4)
  1  .00                         ISTRT THMAX
    .0000     .0000              RD(i) d(i)  Terrain Data Point
    .5000    61.8034             RD(i) d(i)  Terrain Data Point
   1.0000   117.5571             RD(i) d(i)  Terrain Data Point
   1.5000   161.8034             RD(i) d(i)  Terrain Data Point
   2.0000   190.2113             RD(i) d(i)  Terrain Data Point
   2.5000   200.0000             RD(i) d(i)  Terrain Data Point
   3.0000   190.2113             RD(i) d(i)  Terrain Data Point
   3.5000   161.8034             RD(i) d(i)  Terrain Data Point
   4.0000   117.5570             RD(i) d(i)  Terrain Data Point
   4.5000    61.8034             RD(i) d(i)  Terrain Data Point
   5.0000     .0000              RD(i) d(i)  Terrain Data Point
   5.5000   -61.8034             RD(i) d(i)  Terrain Data Point
   6.0000  -117.5571             RD(i) d(i)  Terrain Data Point
   6.5000  -161.8034             RD(i) d(i)  Terrain Data Point
   7.0000  -190.2113             RD(i) d(i)  Terrain Data Point
   7.5000  -200.0000             RD(i) d(i)  Terrain Data Point
   8.0000  -190.2113             RD(i) d(i)  Terrain Data Point
   8.5000  -161.8034             RD(i) d(i)  Terrain Data Point
   9.0000  -117.5570             RD(i) d(i)  Terrain Data Point
   9.5000   -61.8034             RD(i) d(i)  Terrain Data Point
  10.0000     .0000              RD(i) d(i)  Terrain Data Point
  10.5000    61.8034             RD(i) d(i)  Terrain Data Point
  11.0000   117.5571             RD(i) d(i)  Terrain Data Point
  11.5000   161.8034             RD(i) d(i)  Terrain Data Point
  12.0000   190.2113             RD(i) d(i)  Terrain Data Point
  12.5000   200.0000             RD(i) d(i)  Terrain Data Point
  13.0000   190.2113             RD(i) d(i)  Terrain Data Point
  13.5000   161.8034             RD(i) d(i)  Terrain Data Point
  14.0000   117.5570             RD(i) d(i)  Terrain Data Point
  14.5000    61.8034             RD(i) d(i)  Terrain Data Point
  15.0000    -.0001              RD(i) d(i)  Terrain Data Point
  15.5000   -61.8035             RD(i) d(i)  Terrain Data Point
  16.0000  -117.5571             RD(i) d(i)  Terrain Data Point
  16.5000  -161.8034             RD(i) d(i)  Terrain Data Point
  17.0000  -190.2113             RD(i) d(i)  Terrain Data Point
  17.5000  -200.0000             RD(i) d(i)  Terrain Data Point
  18.0000  -190.2113             RD(i) d(i)  Terrain Data Point
  18.5000  -161.8034             RD(i) d(i)  Terrain Data Point
  19.0000  -117.5570             RD(i) d(i)  Terrain Data Point
  19.5000   -61.8033             RD(i) d(i)  Terrain Data Point
  20.0000     .0001              RD(i) d(i)  Terrain Data Point
  20.5000    61.8035             RD(i) d(i)  Terrain Data Point
  21.0000   117.5571             RD(i) d(i)  Terrain Data Point
  21.5000   161.8034             RD(i) d(i)  Terrain Data Point
  22.0000   190.2113             RD(i) d(i)  Terrain Data Point
  22.5000   200.0000             RD(i) d(i)  Terrain Data Point
  23.0000   190.2113             RD(i) d(i)  Terrain Data Point
  23.5000   161.8033             RD(i) d(i)  Terrain Data Point
  24.0000   117.5570             RD(i) d(i)  Terrain Data Point
```

| | | | |
|---|---|---|---|
| 24.5000 | 61.8033 | RD(i) d(i) | Terrain Data Point |
| 25.0000 | -.0001 | RD(i) d(i) | Terrain Data Point |
| 25.5000 | -61.8035 | RD(i) d(i) | Terrain Data Point |
| 26.0000 | -117.5571 | RD(i) d(i) | Terrain Data Point |
| 26.5000 | -161.8035 | RD(i) d(i) | Terrain Data Point |
| 27.0000 | -190.2113 | RD(i) d(i) | Terrain Data Point |
| 27.5000 | -200.0000 | RD(i) d(i) | Terrain Data Point |
| 28.0000 | -190.2113 | RD(i) d(i) | Terrain Data Point |
| 28.5000 | -161.8033 | RD(i) d(i) | Terrain Data Point |
| 29.0000 | -117.5570 | RD(i) d(i) | Terrain Data Point |
| 29.5000 | -61.8033 | RD(i) d(i) | Terrain Data Point |
| 30.0000 | .0001 | RD(i) d(i) | Terrain Data Point |
| 30.5000 | 61.8034 | RD(i) d(i) | Terrain Data Point |
| 31.0000 | 117.5571 | RD(i) d(i) | Terrain Data Point |
| 31.5000 | 161.8034 | RD(i) d(i) | Terrain Data Point |
| 32.0000 | 190.2113 | RD(i) d(i) | Terrain Data Point |
| 32.5000 | 200.0000 | RD(i) d(i) | Terrain Data Point |
| 33.0000 | 190.2113 | RD(i) d(i) | Terrain Data Point |
| 33.5000 | 161.8034 | RD(i) d(i) | Terrain Data Point |
| 34.0000 | 117.5570 | RD(i) d(i) | Terrain Data Point |
| 34.5000 | 61.8034 | RD(i) d(i) | Terrain Data Point |
| 35.0000 | .0000 | RD(i) d(i) | Terrain Data Point |
| 35.5000 | -61.8034 | RD(i) d(i) | Terrain Data Point |
| 36.0000 | -117.5571 | RD(i) d(i) | Terrain Data Point |
| 36.5000 | -161.8034 | RD(i) d(i) | Terrain Data Point |
| 37.0000 | -190.2113 | RD(i) d(i) | Terrain Data Point |
| 37.5000 | -200.0000 | RD(i) d(i) | Terrain Data Point |
| 38.0000 | -190.2113 | RD(i) d(i) | Terrain Data Point |
| 38.5000 | -161.8034 | RD(i) d(i) | Terrain Data Point |
| 39.0000 | -117.5570 | RD(i) d(i) | Terrain Data Point |
| 39.5000 | -61.8034 | RD(i) d(i) | Terrain Data Point |
| 40.0000 | .0000 | RD(i) d(i) | Terrain Data Point |
| 40.5000 | 61.8034 | RD(i) d(i) | Terrain Data Point |
| 41.0000 | 117.5571 | RD(i) d(i) | Terrain Data Point |
| 41.5000 | 161.8034 | RD(i) d(i) | Terrain Data Point |
| 42.0000 | 190.2113 | RD(i) d(i) | Terrain Data Point |
| 42.5000 | 200.0000 | RD(i) d(i) | Terrain Data Point |
| 43.0000 | 190.2113 | RD(i) d(i) | Terrain Data Point |
| 43.5000 | 161.8034 | RD(i) d(i) | Terrain Data Point |
| 44.0000 | 117.5570 | RD(i) d(i) | Terrain Data Point |
| 44.5000 | 61.8034 | RD(i) d(i) | Terrain Data Point |
| 45.0000 | -.0001 | RD(i) d(i) | Terrain Data Point |
| 45.5000 | -61.8035 | RD(i) d(i) | Terrain Data Point |
| 46.0000 | -117.5571 | RD(i) d(i) | Terrain Data Point |
| 46.5000 | -161.8034 | RD(i) d(i) | Terrain Data Point |
| 47.0000 | -190.2113 | RD(i) d(i) | Terrain Data Point |
| 47.5000 | -200.0000 | RD(i) d(i) | Terrain Data Point |
| 48.0000 | -190.2113 | RD(i) d(i) | Terrain Data Point |
| 48.5000 | -161.8034 | RD(i) d(i) | Terrain Data Point |
| 49.0000 | -117.5570 | RD(i) d(i) | Terrain Data Point |
| 49.5000 | -61.8033 | RD(i) d(i) | Terrain Data Point |
| 50.0000 | .0001 | RD(i) d(i) | Terrain Data Point |
| -999 | -999 | | |
| .0000 | 376.0000 | z(i) N(i) | |
| 200.0000 | 300.0000 | z(i) N(i) | |
| 500.0000 | 200.0000 | z(i) N(i) | |
| -999 | -999 | | |
| .0000 | 5.0000 | z(i) EPS(i) | |

```
   -999      -999
  -500.0000    .0100           z(i) SIGMA(i)
  -450.0000    .0010           z(i) SIGMA(i)
  -400.0000    .0001           z(i) SIGMA(i)
     .0000     .0001           z(i) SIGMA(i)
   -999      -999
    5.000000E-01
    61.8034   376.0000          z(i)   N(i)
   261.8034   300.0000          z(i)   N(i)
   561.8034   200.0000          z(i)   N(i)
   -999      -999
    61.8034     5.0000          z(i)  EPS(i)
   -999      -999
  -438.1966    .0100           z(i) SIGMA(i)
  -388.1966    .0010           z(i) SIGMA(i)
  -338.1966    .0001           z(i) SIGMA(i)
    61.8034    .0001           z(i) SIGMA(i)
   -999      -999
    1.000000
   117.5571   376.0000          z(i)   N(i)
   317.5571   300.0000          z(i)   N(i)
   617.5571   200.0000          z(i)   N(i)
   -999      -999
   117.5571     5.0000          z(i)  EPS(i)
   -999      -999
  -382.4429    .0100           z(i) SIGMA(i)
  -332.4429    .0010           z(i) SIGMA(i)
  -282.4429    .0001           z(i) SIGMA(i)
   117.5571    .0001           z(i) SIGMA(i)
   -999      -999
    1.500000
   161.8034   376.0000          z(i)   N(i)
   361.8034   300.0000          z(i)   N(i)
   661.8034   200.0000          z(i)   N(i)
   -999      -999
   161.8034     5.0000          z(i)  EPS(i)
   -999      -999
  -338.1966    .0100           z(i) SIGMA(i)
  -288.1966    .0010           z(i) SIGMA(i)
  -238.1966    .0001           z(i) SIGMA(i)
   161.8034    .0001           z(i) SIGMA(i)
   -999      -999
    2.000000
   190.2113   376.0000          z(i)   N(i)
   390.2113   300.0000          z(i)   N(i)
   690.2113   200.0000          z(i)   N(i)
   -999      -999
   190.2113     5.0000          z(i)  EPS(i)
   -999      -999
  -309.7887    .0100           z(i) SIGMA(i)
  -259.7887    .0010           z(i) SIGMA(i)
  -209.7887    .0001           z(i) SIGMA(i)
   190.2113    .0001           z(i) SIGMA(i)
   -999      -999
    2.500000
   200.0000   376.0000          z(i)   N(i)
   400.0000   300.0000          z(i)   N(i)
   700.0000   200.0000          z(i)   N(i)
```

```
    -999      -999
  200.0000   5.0000              z(i)  EPS(i)
    -999      -999
 -300.0000    .0100              z(i)  SIGMA(i)
 -250.0000    .0010              z(i)  SIGMA(i)
 -200.0000    .0001              z(i)  SIGMA(i)
  200.0000    .0001              z(i)  SIGMA(i)
    -999      -999
     3.000000
  190.2113  376.0000             z(i)   N(i)
  390.2113  300.0000             z(i)   N(i)
  690.2113  200.0000             z(i)   N(i)
    -999      -999
  190.2113    5.0000             z(i)  EPS(i)
    -999      -999
 -309.7887    .0100              z(i)  SIGMA(i)
 -259.7887    .0010              z(i)  SIGMA(i)
 -209.7887    .0001              z(i)  SIGMA(i)
  190.2113    .0001              z(i)  SIGMA(i)
    -999      -999
     3.500000
  161.8034  376.0000             z(i)   N(i)
  361.8034  300.0000             z(i)   N(i)
  661.8034  200.0000             z(i)   N(i)
    -999      -999
  161.8034    5.0000             z(i)  EPS(i)
    -999      -999
 -338.1966    .0100              z(i)  SIGMA(i)
 -288.1966    .0010              z(i)  SIGMA(i)
 -238.1966    .0001              z(i)  SIGMA(i)
  161.8034    .0001              z(i)  SIGMA(i)
    -999      -999
     4.000000
  117.5570  376.0000             z(i)   N(i)
  317.5570  300.0000             z(i)   N(i)
  617.5570  200.0000             z(i)   N(i)
    -999      -999
  117.5570    5.0000             z(i)  EPS(i)
    -999      -999
 -382.4430    .0100              z(i)  SIGMA(i)
 -332.4430    .0010              z(i)  SIGMA(i)
 -282.4430    .0001              z(i)  SIGMA(i)
  117.5570    .0001              z(i)  SIGMA(i)
    -999      -999
     4.500000
   61.8034  376.0000             z(i)   N(i)
  261.8034  300.0000             z(i)   N(i)
  561.8034  200.0000             z(i)   N(i)
    -999      -999
   61.8034    5.0000             z(i)  EPS(i)
    -999      -999
 -438.1966    .0100              z(i)  SIGMA(i)
 -388.1966    .0010              z(i)  SIGMA(i)
 -338.1966    .0001              z(i)  SIGMA(i)
   61.8034    .0001              z(i) SIGMA(i)
    -999      -999
     5.000000
    .0000   376.0000             z(i)   N(i)
```

```
 200.0000  300.0000            z(i)   N(i)
 500.0000  200.0000            z(i)   N(i)
 -999      -999
   .0000    5.0000         z(i)  EPS(i)
 -999      -999
-500.0000    .0100         z(i)  SIGMA(i)
-450.0000    .0010         z(i)  SIGMA(i)
-400.0000    .0001         z(i)  SIGMA(i)
   .0000    .0001       z(i)  SIGMA(i)
 -999      -999
   5.500000
 -61.8034  376.0000          z(i)   N(i)
 138.1966  300.0000          z(i)   N(i)
 438.1966  200.0000          z(i)   N(i)
 -999      -999
 -61.8034    5.0000        z(i)  EPS(i)
 -999      -999
-561.8034    .0100         z(i)  SIGMA(i)
-511.8034    .0010         z(i)  SIGMA(i)
-461.8034    .0001         z(i)  SIGMA(i)
 -61.8034    .0001       z(i)  SIGMA(i)
 -999      -999
   6.000000
-117.5571  376.0000          z(i)   N(i)
  82.4429  300.0000         z(i)   N(i)
 382.4429  200.0000          z(i)   N(i)
 -999      -999
-117.5571    5.0000        z(i)  EPS(i)
 -999      -999
-617.5571    .0100         z(i)  SIGMA(i)
-567.5571    .0010         z(i)  SIGMA(i)
-517.5571    .0001         z(i)  SIGMA(i)
-117.5571    .0001         z(i)  SIGMA(i)
 -999      -999
   6.500000
-161.8034  376.0000          z(i)   N(i)
  38.1966  300.0000         z(i)   N(i)
 338.1966  200.0000          z(i)   N(i)
 -999      -999
-161.8034    5.0000        z(i)  EPS(i)
 -999      -999
-661.8034    .0100         z(i)  SIGMA(i)
-611.8034    .0010         z(i)  SIGMA(i)
-561.8034    .0001         z(i)  SIGMA(i)
-161.8034    .0001         z(i)  SIGMA(i)
 -999      -999
   7.000000
-190.2113  376.0000          z(i)   N(i)
   9.7887  300.0000         z(i)   N(i)
 309.7887  200.0000          z(i)   N(i)
 -999      -999
-190.2113    5.0000        z(i)  EPS(i)
 -999      -999
-690.2113    .0100         z(i)  SIGMA(i)
-640.2113    .0010         z(i)  SIGMA(i)
-590.2113    .0001         z(i)  SIGMA(i)
-190.2113    .0001         z(i)  SIGMA(i)
 -999      -999
```

```
        7.500000
-200.0000  376.0000              z(i)   N(i)
      .0000  300.0000            z(i)   N(i)
  300.0000  200.0000             z(i)   N(i)
     -999     -999
-200.0000    5.0000              z(i)  EPS(i)
     -999     -999
-700.0000     .0100              z(i) SIGMA(i)
-650.0000     .0010              z(i) SIGMA(i)
-600.0000     .0001              z(i) SIGMA(i)
-200.0000     .0001              z(i) SIGMA(i)
     -999     -999
        8.000000
-190.2113  376.0000              z(i)   N(i)
    9.7887  300.0000             z(i)   N(i)
  309.7887  200.0000             z(i)   N(i)
     -999     -999
-190.2113    5.0000              z(i)  EPS(i)
     -999     -999
-690.2113     .0100              z(i) SIGMA(i)
-640.2113     .0010              z(i) SIGMA(i)
-590.2113     .0001              z(i) SIGMA(i)
-190.2113     .0001              z(i) SIGMA(i)
     -999     -999
        8.500000
-161.8034  376.0000              z(i)   N(i)
   38.1966  300.0000             z(i)   N(i)
  338.1966  200.0000             z(i)   N(i)
     -999     -999
-161.8034    5.0000              z(i)  EPS(i)
     -999     -999
-661.8033     .0100              z(i) SIGMA(i)
-611.8033     .0010              z(i) SIGMA(i)
-561.8033     .0001              z(i) SIGMA(i)
-161.8034     .0001              z(i) SIGMA(i)
     -999     -999
        9.000000
-117.5570  376.0000              z(i)   N(i)
   82.4430  300.0000             z(i)   N(i)
  382.4430  200.0000             z(i)   N(i)
     -999     -999
-117.5570    5.0000              z(i)  EPS(i)
     -999     -999
-617.5570     .0100              z(i) SIGMA(i)
-567.5570     .0010              z(i) SIGMA(i)
-517.5570     .0001              z(i) SIGMA(i)
-117.5570     .0001              z(i) SIGMA(i)
     -999     -999
        9.500000
-61.8034   376.0000              z(i)   N(i)
  138.1966  300.0000             z(i)   N(i)
  438.1966  200.0000             z(i)   N(i)
     -999     -999
-61.8034     5.0000              z(i)  EPS(i)
     -999     -999
-561.8033     .0100              z(i) SIGMA(i)
-511.8034     .0010              z(i) SIGMA(i)
-461.8034     .0001              z(i) SIGMA(i)
```

```
-61.8034    .0001            z(i) SIGMA(i)
 -999      -999
     10.000000
    .0000  376.0000          z(i)  N(i)
200.0000  300.0000            z(i)  N(i)
500.0000  200.0000            z(i)  N(i)
 -999      -999
    .0000   5.0000           z(i) EPS(i)
 -999      -999
-500.0000    .0100            z(i) SIGMA(i)
-450.0000    .0010            z(i) SIGMA(i)
-400.0000    .0001            z(i) SIGMA(i)
    .0000    .0001           z(i) SIGMA(i)
 -999      -999
     10.500000
 61.8034  376.0000            z(i)  N(i)
261.8034  300.0000            z(i)  N(i)
561.8034  200.0000            z(i)  N(i)
 -999      -999
 61.8034   5.0000            z(i) EPS(i)
 -999      -999
-438.1966    .0100            z(i) SIGMA(i)
-388.1966    .0010            z(i) SIGMA(i)
-338.1966    .0001            z(i) SIGMA(i)
 61.8034    .0001            z(i) SIGMA(i)
 -999      -999
     11.000000
117.5571  376.0000            z(i)  N(i)
317.5571  300.0000            z(i)  N(i)
617.5571  200.0000            z(i)  N(i)
 -999      -999
117.5571   5.0000            z(i) EPS(i)
 -999      -999
-382.4429    .0100            z(i) SIGMA(i)
-332.4429    .0010            z(i) SIGMA(i)
-282.4429    .0001            z(i) SIGMA(i)
117.5571    .0001            z(i) SIGMA(i)
 -999      -999
     11.500000
161.8034  376.0000            z(i)  N(i)
361.8034  300.0000            z(i)  N(i)
661.8034  200.0000            z(i)  N(i)
 -999      -999
161.8034   5.0000            z(i) EPS(i)
 -999      -999
-338.1966    .0100            z(i) SIGMA(i)
-288.1966    .0010            z(i) SIGMA(i)
-238.1966    .0001            z(i) SIGMA(i)
161.8034    .0001            z(i) SIGMA(i)
 -999      -999
     12.000000
190.2113  376.0000            z(i)  N(i)
390.2113  300.0000            z(i)  N(i)
690.2113  200.0000            z(i)  N(i)
 -999      -999
190.2113   5.0000            z(i) EPS(i)
 -999      -999
-309.7887    .0100            z(i) SIGMA(i)
```

```
-259.7887    .0010          z(i)  SIGMA(i)
-209.7887    .0001          z(i)  SIGMA(i)
 190.2113    .0001          z(i)  SIGMA(i)
   -999     -999
    12.500000
 200.0000  376.0000          z(i)   N(i)
 400.0000  300.0000          z(i)   N(i)
 700.0000  200.0000          z(i)   N(i)
   -999     -999
 200.0000    5.0000          z(i)  EPS(i)
   -999     -999
-300.0000    .0100          z(i)  SIGMA(i)
-250.0000    .0010          z(i)  SIGMA(i)
-200.0000    .0001          z(i)  SIGMA(i)
 200.0000    .0001          z(i)  SIGMA(i)
   -999     -999
    13.000000
 190.2113  376.0000          z(i)   N(i)
 390.2113  300.0000          z(i)   N(i)
 690.2113  200.0000          z(i)   N(i)
   -999     -999
 190.2113    5.0000          z(i)  EPS(i)
   -999     -999
-309.7887    .0100          z(i)  SIGMA(i)
-259.7887    .0010          z(i)  SIGMA(i)
-209.7887    .0001          z(i)  SIGMA(i)
 190.2113    .0001          z(i)  SIGMA(i)
   -999     -999
    13.500000
 161.8034  376.0000          z(i)   N(i)
 361.8034  300.0000          z(i)   N(i)
 661.8033  200.0000          z(i)   N(i)
   -999     -999
 161.8034    5.0000          z(i)  EPS(i)
   -999     -999
-338.1966    .0100          z(i)  SIGMA(i)
-288.1966    .0010          z(i)  SIGMA(i)
-238.1966    .0001          z(i)  SIGMA(i)
 161.8034    .0001          z(i)  SIGMA(i)
   -999     -999
    14.000000
 117.5570  376.0000          z(i)   N(i)
 317.5570  300.0000          z(i)   N(i)
 617.5570  200.0000          z(i)   N(i)
   -999     -999
 117.5570    5.0000          z(i)  EPS(i)
   -999     -999
-382.4430    .0100          z(i)  SIGMA(i)
-332.4430    .0010          z(i)  SIGMA(i)
-282.4430    .0001          z(i)  SIGMA(i)
 117.5570    .0001          z(i)  SIGMA(i)
   -999     -999
    14.500000
  61.8034  376.0000          z(i)   N(i)
 261.8033  300.0000          z(i)   N(i)
 561.8033  200.0000          z(i)   N(i)
   -999     -999
  61.8034    5.0000          z(i)  EPS(i)
```

```
  -999      -999
-438.1967     .0100        z(i) SIGMA(i)
-388.1967     .0010        z(i) SIGMA(i)
-338.1967     .0001        z(i) SIGMA(i)
  61.8034     .0001        z(i) SIGMA(i)
  -999      -999
   15.000000
  -.0001  376.0000         z(i)  N(i)
 200.0000  300.0000          z(i)  N(i)
 499.9999  200.0000          z(i)  N(i)
  -999      -999
  -.0001    5.0000          z(i)  EPS(i)
  -999      -999
-500.0001     .0100          z(i) SIGMA(i)
-450.0001     .0010          z(i) SIGMA(i)
-400.0001     .0001          z(i) SIGMA(i)
  -.0001     .0001        z(i) SIGMA(i)
  -999      -999
   15.500000
 -61.8035  376.0000          z(i)  N(i)
 138.1965  300.0000          z(i)  N(i)
 438.1965  200.0000          z(i)  N(i)
  -999      -999
 -61.8035    5.0000          z(i)  EPS(i)
  -999      -999
-561.8035     .0100          z(i) SIGMA(i)
-511.8035     .0010          z(i) SIGMA(i)
-461.8035     .0001          z(i) SIGMA(i)
 -61.8035     .0001          z(i) SIGMA(i)
  -999      -999
   16.000000
-117.5571  376.0000          z(i)  N(i)
  82.4429  300.0000          z(i)  N(i)
 382.4429  200.0000          z(i)  N(i)
  -999      -999
-117.5571    5.0000          z(i)  EPS(i)
  -999      -999
-617.5571     .0100          z(i) SIGMA(i)
-567.5571     .0010          z(i) SIGMA(i)
-517.5571     .0001          z(i) SIGMA(i)
-117.5571     .0001          z(i) SIGMA(i)
  -999      -999
   16.500000
-161.8034  376.0000          z(i)  N(i)
  38.1966  300.0000          z(i)  N(i)
 338.1966  200.0000          z(i)  N(i)
  -999      -999
-161.8034    5.0000          z(i)  EPS(i)
  -999      -999
-661.8035     .0100          z(i) SIGMA(i)
-611.8035     .0010          z(i) SIGMA(i)
-561.8035     .0001          z(i) SIGMA(i)
-161.8034     .0001          z(i) SIGMA(i)
  -999      -999
   17.000000
-190.2113  376.0000          z(i)  N(i)
   9.7887  300.0000          z(i)  N(i)
 309.7887  200.0000          z(i)  N(i)
```

```
  -999      -999
-190.2113    5.0000              z(i)  EPS(i)
  -999      -999
-690.2113    .0100              z(i)  SIGMA(i)
-640.2113    .0010              z(i)  SIGMA(i)
-590.2113    .0001              z(i)  SIGMA(i)
-190.2113    .0001              z(i)  SIGMA(i)
  -999      -999
   17.500000
-200.0000  376.0000              z(i)   N(i)
   .0000  300.0000              z(i)   N(i)
 300.0000  200.0000              z(i)   N(i)
  -999      -999
-200.0000    5.0000              z(i)  EPS(i)
  -999      -999
-700.0000    .0100              z(i)  SIGMA(i)
-650.0000    .0010              z(i)  SIGMA(i)
-600.0000    .0001              z(i)  SIGMA(i)
-200.0000    .0001              z(i)  SIGMA(i)
  -999      -999
   18.000000
-190.2113  376.0000              z(i)   N(i)
   9.7887  300.0000              z(i)   N(i)
 309.7887  200.0000              z(i)   N(i)
  -999      -999
-190.2113    5.0000              z(i)  EPS(i)
  -999      -999
-690.2113    .0100              z(i)  SIGMA(i)
-640.2113    .0010              z(i)  SIGMA(i)
-590.2113    .0001              z(i)  SIGMA(i)
-190.2113    .0001              z(i)  SIGMA(i)
  -999      -999
   18.500000
-161.8034  376.0000              z(i)   N(i)
  38.1966  300.0000              z(i)   N(i)
 338.1967  200.0000              z(i)   N(i)
  -999      -999
-161.8034    5.0000              z(i)  EPS(i)
  -999      -999
-661.8033    .0100              z(i)  SIGMA(i)
-611.8033    .0010              z(i)  SIGMA(i)
-561.8033    .0001              z(i)  SIGMA(i)
-161.8034    .0001              z(i)  SIGMA(i)
  -999      -999
   19.000000
-117.5570  376.0000              z(i)   N(i)
  82.4430  300.0000              z(i)   N(i)
 382.4430  200.0000              z(i)   N(i)
  -999      -999
-117.5570    5.0000              z(i)  EPS(i)
  -999      -999
-617.5570    .0100              z(i)  SIGMA(i)
-567.5570    .0010              z(i)  SIGMA(i)
-517.5570    .0001              z(i)  SIGMA(i)
-117.5570    .0001              z(i)  SIGMA(i)
  -999      -999
   19.500000
 -61.8033  376.0000              z(i)   N(i)
```

```
138.1967  300.0000              z(i)  N(i)
438.1967  200.0000              z(i)  N(i)
-999      -999
-61.8033    5.0000              z(i)  EPS(i)
-999      -999
-561.8033   .0100               z(i)  SIGMA(i)
-511.8033   .0010               z(i)  SIGMA(i)
-461.8033   .0001               z(i)  SIGMA(i)
-61.8033    .0001               z(i)  SIGMA(i)
-999      -999
  20.000000
   .0001  376.0000              z(i)  N(i)
200.0001  300.0000              z(i)  N(i)
500.0001  200.0000              z(i)  N(i)
-999      -999
  .0001    5.0000               z(i)  EPS(i)
-999      -999
-499.9999   .0100               z(i)  SIGMA(i)
-449.9999   .0010               z(i)  SIGMA(i)
-399.9999   .0001               z(i)  SIGMA(i)
   .0001    .0001               z(i)  SIGMA(i)
-999      -999
  20.500000
 61.8035  376.0000              z(i)  N(i)
261.8035  300.0000              z(i)  N(i)
561.8035  200.0000              z(i)  N(i)
-999      -999
 61.8035    5.0000              z(i)  EPS(i)
-999      -999
-438.1965   .0100               z(i)  SIGMA(i)
-388.1965   .0010               z(i)  SIGMA(i)
-338.1965   .0001               z(i)  SIGMA(i)
 61.8035    .0001               z(i)  SIGMA(i)
-999      -999
  21.000000
117.5571  376.0000              z(i)  N(i)
317.5571  300.0000              z(i)  N(i)
617.5571  200.0000              z(i)  N(i)
-999      -999
117.5571    5.0000              z(i)  EPS(i)
-999      -999
-382.4429   .0100               z(i)  SIGMA(i)
-332.4429   .0010               z(i)  SIGMA(i)
-282.4429   .0001               z(i)  SIGMA(i)
117.5571    .0001               z(i)  SIGMA(i)
-999      -999
  21.500000
161.8034  376.0000              z(i)  N(i)
361.8034  300.0000              z(i)  N(i)
661.8035  200.0000              z(i)  N(i)
-999      -999
161.8034    5.0000              z(i)  EPS(i)
-999      -999
-338.1966   .0100               z(i)  SIGMA(i)
-288.1966   .0010               z(i)  SIGMA(i)
-238.1966   .0001               z(i)  SIGMA(i)
161.8034    .0001               z(i)  SIGMA(i)
-999      -999
```

```
     22.000000
190.2113  376.0000              z(i)  N(i)
390.2113  300.0000              z(i)  N(i)
690.2113  200.0000              z(i)  N(i)
  -999    -999
190.2113    5.0000              z(i)  EPS(i)
  -999    -999
-309.7887   .0100               z(i)  SIGMA(i)
-259.7887   .0010               z(i)  SIGMA(i)
-209.7887   .0001               z(i)  SIGMA(i)
190.2113    .0001               z(i)  SIGMA(i)
  -999    -999
     22.500000
200.0000  376.0000              z(i)  N(i)
400.0000  300.0000              z(i)  N(i)
700.0000  200.0000              z(i)  N(i)
  -999    -999
200.0000    5.0000              z(i)  EPS(i)
  -999    -999
-300.0000   .0100               z(i)  SIGMA(i)
-250.0000   .0010               z(i)  SIGMA(i)
-200.0000   .0001               z(i)  SIGMA(i)
200.0000    .0001               z(i)  SIGMA(i)
  -999    -999
     23.000000
190.2113  376.0000              z(i)  N(i)
390.2113  300.0000              z(i)  N(i)
690.2113  200.0000              z(i)  N(i)
  -999    -999
190.2113    5.0000              z(i)  EPS(i)
  -999    -999
-309.7887   .0100               z(i)  SIGMA(i)
-259.7887   .0010               z(i)  SIGMA(i)
-209.7887   .0001               z(i)  SIGMA(i)
190.2113    .0001               z(i)  SIGMA(i)
  -999    -999
     23.500000
161.8033  376.0000              z(i)  N(i)
361.8033  300.0000              z(i)  N(i)
661.8033  200.0000              z(i)  N(i)
  -999    -999
161.8033    5.0000              z(i)  EPS(i)
  -999    -999
-338.1967   .0100               z(i)  SIGMA(i)
-288.1967   .0010               z(i)  SIGMA(i)
-238.1967   .0001               z(i)  SIGMA(i)
161.8033    .0001               z(i)  SIGMA(i)
  -999    -999
     24.000000
117.5570  376.0000              z(i)  N(i)
317.5570  300.0000              z(i)  N(i)
617.5570  200.0000              z(i)  N(i)
  -999    -999
117.5570    5.0000              z(i)  EPS(i)
  -999    -999
-382.4430   .0100               z(i)  SIGMA(i)
-332.4430   .0010               z(i)  SIGMA(i)
-282.4430   .0001               z(i)  SIGMA(i)
```

```
117.5570    .0001            z(i)  SIGMA(i)
 -999     -999
   24.500000
 61.8033  376.0000           z(i)   N(i)
261.8033  300.0000            z(i)   N(i)
561.8033  200.0000            z(i)   N(i)
 -999     -999
 61.8033    5.0000           z(i)  EPS(i)
 -999     -999
-438.1967    .0100           z(i)  SIGMA(i)
-388.1967    .0010           z(i)  SIGMA(i)
-338.1967    .0001           z(i)  SIGMA(i)
 61.8033    .0001            z(i)  SIGMA(i)
 -999     -999
```

Example 2 Output
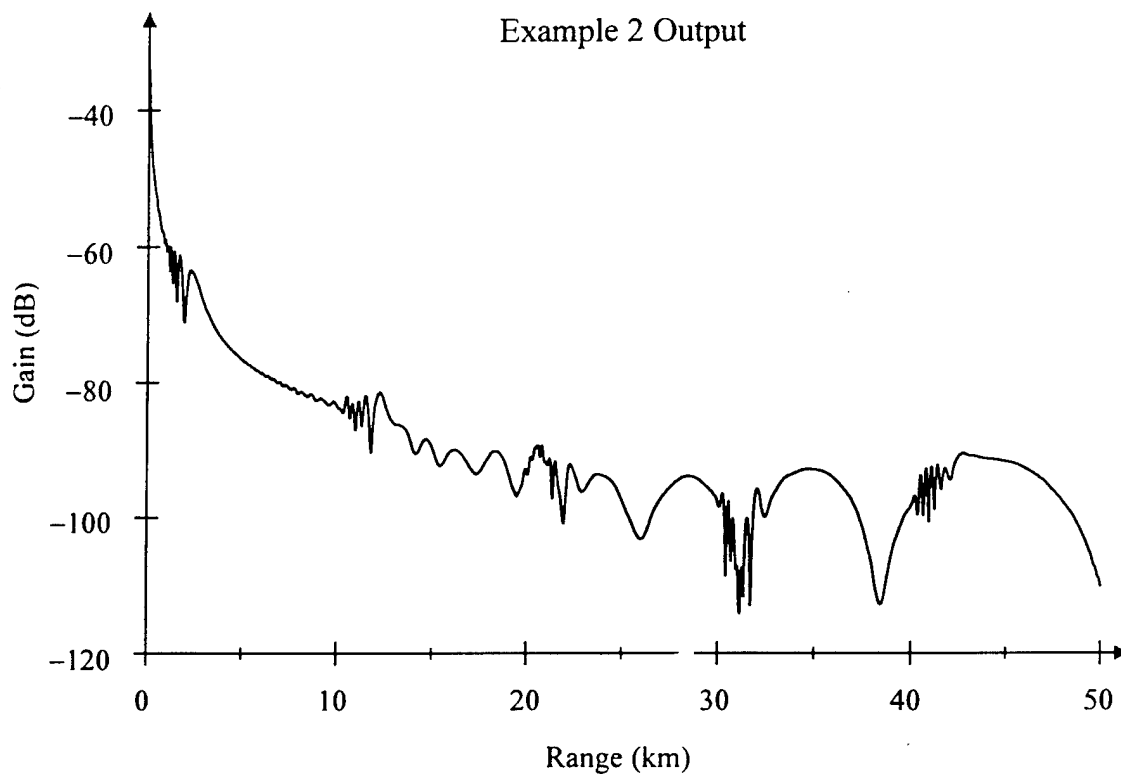


Figure 4

Good luck, and please inform me of any problems you may have.  I can be reached at

Work
UMass Lowell
Dept. of Mathematical Sciences
1 University Ave.
Lowell, MA 01854
978-934-2440 (Phone)
978-934-3053 (Fax)
Ronald_Brent@uml.edu

Home
36A St. Paul St.  #2
Brookline, MA 01854
617-566-3089
RB733@aol.com

# References

1. Brent Ronald I. and Joseph F. A. Ormsby, "Scalar electromagnetic propagation modeling using parabolic equations and the split-step Pade approximation," J. Phys. A: Math. Gen. **28** 2065-2080 (1995)

2. Collins Michael D. "A split-step Pade solution for the parabolic equation method," J. Acoust. Soc. Am. **93**(4), pp. 1736-1742, 1993.

3. Collins Michael D. " A two-way parabolic equation for acoustic backscatter in the ocean," J. Acoust. Soc. Am **91**(4), pp. 1357-1368, 1992.

**Appendix A**
**Reference 1**

# Scalar electromagnetic propagation modelling using parabolic equations and the split-step Padé approximation

Ronald I Brent† and Joseph F A Ormsby‡

† Department of Mathematical Sciences, University of Massachusetts Lowell, Lowell, MA 01854, USA
‡ Joint Command and Control Warfare Center, Kelly AFB, San Antonio TX 78243, USA

**Abstract.** This paper presents a solution of 2D electromagnetic wave propagation problems in complicated terrestrial domains. Scalar 2D parabolic approximations are derived from Maxwell's equations for both vertical and horizontal polarization. The parabolic equations are then solved using a new technique involving Padé rational function approximations of the macroscopic operator. This method allows for larger-than-normal range stepping, speeding up computational time significantly. The Padé approximation and the numerical implementation are fully discussed. The discontinuity at the earth's surface is handled directly by using classical continuity conditions and deriving exact interface conditions for linking the fields in the atmosphere to those in the terrain. The interface conditions are then implemented using the concept of virtual points. Preliminary benchmark tests show the interface treatment to work well. Finally, several example runs are presented illustrating results.

## 1. Introduction

The solution of electromagnetic (EM) propagation problems in the terrestrial domain is a complicated matter. Three-dimensional (3D) variations in refraction and terrain make the full vector problem extremely difficult to solve in reasonable time. If one chooses to simplify the problem by assuming symmetry in one or more of the coordinate directions, the vector problem can be uncoupled into two scalar problems [1]. However, the solution of the two-dimensional (2D) scalar problem is still very difficult for realistic environments. The parabolic approximation method is used to reduce the solution of the full two-way wave equation to a solution of a one-way equation [2]. Benefits of one-way propagation are the simple numerical implementation of range dependencies in the medium, and the avoidance of prohibitive numerical aspects of solving elliptic equations associated with implementing two range-dependent boundary conditions. The model discussed in this paper is a so called 2.5D model using azimuthally varied vertical planar fields. Work is also proceeding on a 3D model for higher frequencies using a hybrid combination of an underlying robust 3D ray trace and a 3D Gaussian beam model.

Two of the most popular methods of solving the parabolic equations are the implicit finite difference (IFD) method [3] and the split-step Fourier transform method [4, 5]. These techniques are microscopic methods in the sense that they are implementing approximations to the differential equation, defined microscopically. Limitations of these methods are that the grid mesh over which the solution is computed must be small to yield accuracy. This often means grid sizes on the scale of at most three wavelengths. At high frequencies and large propagation domains this could amount to grid sizes of hundreds of thousands by

millions of points needed for an accurate solution. Methods using fourth-order difference schemes have also been implemented to speed up computational time [6]. A better method to solve the equations is by symbolically integrating the equation with respect to range thereby obtaining the macroscopic propagator [7]. In theory if one does an 'infinitely' good job at approximating the macroscopic propagator it is possible to take 'infinitely' large range steps. Limitations in adequate range-dependent representation of the macroscopic operator, however, will limit actual range step sizes. In practice one still can achieve great savings in computational time over IFD and even possibly the split-step Fourier transform.

The macroscopic operator is approximated using a Padé rational function series. The more terms used in the approximation, theoretically the larger the range-step one can take. Another advantage of this method is that once the Padé approximation for the propagator has been obtained computations may be applied in parallel. That is, each of the $n$ Padé approximations may be applied to the field at the same time as opposed to having to apply a series of products of operators sequentially. For cases when the desired result is the loss values only near the receiver, and not at many points in-between the source and receiver, the Padé technique applied to the macroscopic operator is ideal. It cuts down the number of intermediate range locations at which the field must be computed. It is reiterated, however, that the terrain elevation and cover will ultimately determine the range step size.

This report summarizes the theory involved in deriving parabolic approximations to scalar EM propagation and the associated boundary modelling, including energy conservation at vertical interfaces. Also presented is the theory behind the Padé rational function approximation to the propagator, and the complete numerical implementation used in the code SSP. We first begin with the derivation of scalar wave equations for EM propagation.

## 2. Derivation of scalar wave equations

We begin with Maxwell's equations [1] in spherical coordinates $(r, \theta, \phi)$, for terrestrial systems where $r$ is the radial distance from the origin, $\theta$ (measured positive down,) is the angle between the $z$-axis and the radial direction and $\phi$ is the azimuthal angle. Maintaining $E$ planar in the $(r, \theta)$ plane leads to $\partial_\phi H = \partial_\phi \varepsilon = 0$ for vertical polarization and $H$ planar in the $(r, \theta)$ plane leads to $\partial_\phi E = \partial_\phi \varepsilon = 0$ for horizontal polarization. The assumption of symmetry in the $\phi$ direction is a necessary requirement to reduce the original vector problem to uncoupled scalar problems.

These assumptions used in Maxwell's equations readily lead to the two equations

$$\frac{n^2}{r} \frac{\partial}{\partial r} \left( \frac{1}{n^2} \frac{\partial}{\partial r} (r H_\phi) \right) + \frac{n^2}{r^2 \sin \theta} \frac{\partial}{\partial \theta} \left( \frac{\sin \theta}{n^2} \frac{\partial H_\phi}{\partial \theta} \right) + \left( k_0^2 n^2 - \frac{1}{r^2 \sin^2 \theta} - \frac{\cot \theta}{r^2 n^2} \frac{\partial n^2}{\partial \theta} \right) H_\phi = 0$$

$$(1a)$$

and

$$\frac{1}{r} \frac{\partial^2}{\partial r^2} (r E_\phi) + \frac{1}{r^2 \sin \theta} \frac{\partial}{\partial \theta} \left( \sin \theta \frac{\partial E_\phi}{\partial \theta} \right) + \left( k_0^2 n^2 - \frac{1}{r^2 \sin^2 \theta} \right) E_\phi = 0 \quad (1b)$$

where $n$ is the index of refraction defined as

$$n^2 = \frac{\varepsilon}{\varepsilon_0} = \left( \frac{c_0}{c} \right)^2 + \frac{i\sigma}{\omega \varepsilon_0}. \tag{1c}$$

Equation (1*a*) determines the only non-zero component of *H* in the vertical polarization case. Components of *E* are determined in terms of $H_\phi$ using Maxwell's equations. Similarly, equation (1*b*) determines the non-zero component of *E* in the horizontal polarization case. Components of *H* can then be determined in terms of $E_\phi$ using Maxwell's equations. This last equation (1*c*) reflects the inclusion of conductivity via current density terms retained in Maxwell's equations.

One may transform equations (1*a*) and (1*b*) into Helmholtz forms by using the substitutions

$$H_\phi = \frac{nu_V}{\sqrt{r \sin\theta}} \qquad \text{and} \qquad E_\phi = \frac{u_H}{\sqrt{r \sin\theta}}. \tag{2a, b}$$

In doing so, equation (1) yields

$$\frac{1}{r}\frac{\partial}{\partial r}\left(r\frac{\partial u_i}{\partial r}\right) + \frac{1}{r^2}\frac{\partial^2 u_i}{\partial\theta^2} + \left(k_0^2 n^2 - \frac{3}{4r^2 \sin^2\theta} + \delta n_i\right)u_i = 0 \tag{3a}$$

where

$$\delta n_i = \begin{cases} -\dfrac{\cot\theta}{r^2 n}\dfrac{\partial n}{\partial\theta} - \dfrac{n}{r^2}\dfrac{\partial^2 n^{-1}}{\partial\theta^2} - n\dfrac{\partial^2 n^{-1}}{\partial r^2} & \text{for } i \equiv V \\ 0 & \text{for } i \equiv H. \end{cases} \tag{3b}$$

We use the subscript notation $i \equiv V (i \equiv H)$ to denote the vertical (horizontal) polarization.

Since the computation of rectangular domains is more desirable than spherical domains, we now present an 'earth-flattening' approximation to our problem. We will use the smooth earth transformation

$$x = r_e\theta \qquad \text{and} \qquad z = r_e \ln\left(\frac{r}{r_e}\right) \tag{4a, b}$$

where $r_e$ is the radius of the earth at mean sea level (approximately 6370 km). This transformation places the smooth earth's surface at $z = 0$. Terrain will be imposed later during the numerical implementation of the solution algorithm. The inverse transform is given by

$$r = r_e \exp\left(\frac{z}{r_e}\right) \qquad \text{and} \qquad \theta = \frac{x}{r_e}. \tag{5a, b}$$

In using the transformation defined in equation (4) differential operators translate as

$$\frac{\partial}{\partial\theta} \rightarrow r_e\frac{\partial}{\partial x} \qquad \text{and} \qquad \frac{\partial}{\partial r} \rightarrow \exp\left(-\frac{z}{r_e}\right)\frac{\partial}{\partial z}. \tag{6a, b}$$

Equation (3) thereby becomes

$$\frac{\partial^2 u_i}{\partial x^2} + \frac{\partial^2 u_i}{\partial z^2} + \left(k_0^2 m^2 - \frac{3\cosec^2(x/r_e)}{4r_e^2} - \delta m_i\right)u_i = 0 \tag{7a}$$

where *m* is a modified index of refraction defined as

$$m = n \exp\left(\frac{z}{r_e}\right) \tag{7b}$$

A3

and

$$\delta m_i = \begin{cases} -\dfrac{\cot(x/r_e)}{r_e m}\dfrac{\partial m}{\partial x} - m\dfrac{\partial^2 m^{-1}}{\partial x^2} - \dfrac{m}{r_e}\dfrac{\partial m^{-1}}{\partial z} - m\dfrac{\partial^2 m^{-1}}{\partial z^2} & i \equiv V \\ 0 & i \equiv H. \end{cases} \tag{7c}$$

The solution of equation (7a) using parabolic approximation techniques relies on segmenting the medium into a series of range independent sectors. It can be shown that in each of these sectors equation (7a) becomes

$$\frac{\partial^2 u_i}{\partial x^2} + \frac{\partial^2 u_i}{\partial z^2} + K_i^2 u_i = 0 \tag{8a}$$

where

$$K_i^2 = \begin{cases} k_0^2 m^2 - \dfrac{m}{r_e}\dfrac{\partial m^{-1}}{\partial z} - m\dfrac{\partial^2 m^{-1}}{\partial z^2} & i \equiv V \\ k_0^2 m^2 & i \equiv H \end{cases} \tag{8b}$$

and the assumption of $z/r_e \ll 1$ is used. We have also neglected the range-dependent $\cosec^2(*)$ term by assuming we are in the far field $k_0 r \gg 1$ and removed from any poles of the cosecant function $(x < \pi r_e)$ [8]. Equation (8) is the desired starting equation for numerical implementation. We remark that modelling of media with finite conductivity is achieved by replacing $m^2$ with the expression

$$m^2 = \left(\frac{c_0}{c_m}\right)^2 + \frac{i\sigma_m}{\omega\varepsilon_0} \tag{9a}$$

where $c_m$ and $\sigma_m$ are modified light speed and conductivity defined as

$$c_m = c\exp(-z/r_e) \qquad \text{and} \qquad \sigma_m = \sigma\exp(2z/r_e). \tag{9b, c}$$

The next section will discuss the boundary modelling including the effects and corrections for discontinuities in range.

## 3. Electromagnetic boundary modelling

Since we are solving a parabolic equation with two $z$ derivatives and one $x$ derivative, we need two conditions in $z$ and one condition in $x$ at every range step. Computationally we will bound the domain by two horizontal planes at the top of the atmosphere and the bottom of the terrain. Homogeneous Dirichlet conditions will be used at these boundaries and techniques will be applied to reduce fictitious reflections. The fact that the terrain introduces a discontinuity in the problem, and its elevation is range dependent, complicates the problem slightly. Parabolic approximations assume that range-dependent environments are partitioned into range-independent sectors. The result is that terrain slopes are approximated by a series of step-like structures. This creates a vertical interface at each range step where the terrain elevation is altered significantly enough. Typically, the condition at vertical interfaces is continuity of field, however this is not the best condition one might impose

We will eventually impose a conservation of energy condition at discontinuities in range to correct for some range-dependent errors.

We first discuss the modelling of the horizontal interface between the atmosphere and the earth's surface. Assuming finite conductivity and no surface charge density the conditions on $B$, $H$, $D$ and $E$, at an interface between two different media ($\varepsilon_a$, $\mu_a$, $\sigma_a$) and ($\varepsilon_b$, $\mu_b$, $\sigma_b$) are given in [1]. In the case of a smooth interface, the normal vector $e_n = e_r$. Assuming also that magnetic permeability in the terrain is that of the atmosphere (both equal to the free space value,) these conditions imply the following six relations hold:

$$E_{\phi a} = E_{\phi b} \qquad E_{\theta a} = E_{\theta b} \qquad E_{ra} = \frac{\varepsilon_b}{\varepsilon_a} E_{rb} \qquad (10a, b, c)$$

$$H_{\phi a} = H_{\phi b} \qquad H_{\theta a} = H_{\theta b} \quad \text{and} \quad H_{ra} = H_{rb}. \qquad (10d, e, f)$$

For efficient numerical computation, the approach here treats the variable terrain as a series of discrete vertical jumps, i.e. a staircase approximation, using smooth earth formulae for the horizontal boundary conditions in each sector. However, the general boundary conditions for the variable terrain have been determined for vertical and horizontal polarization. The implementation of the general conditions is being examined.

For the case of vertical polarization, clearly one condition on $H_\phi$ is given by equation (10d). The second condition may be obtained by manipulating Maxwell's equations and equation (10b) yielding

$$\frac{1}{\varepsilon_a} \frac{\partial}{\partial r}(r H_{\phi a}) = \frac{1}{\varepsilon_b} \frac{\partial}{\partial r}(r H_{\phi b}) \qquad (11)$$

at the terrain surface. A third condition is also given by $\partial H_{\phi a}/\partial \theta = \partial H_{\phi b}/\partial \theta$ although this will not be used. For the case of horizontal polarization, equation (10a) will be one condition, and the second is obtained by manipulating Maxwell's equations and equation (10e) giving

$$\frac{\partial}{\partial r}(r E_{\phi a}) = \frac{\partial}{\partial r}(r E_{\phi b}) \qquad (12)$$

at the terrain surface. The reason that the horizontal polarization case 'does not see' a discontinuity is because there is, in fact, no discontinuity in permeability at the surface.

We next use the flattening transformation defined in equations (4), and equations (11) and (12) to give

$$\frac{1}{\varepsilon_a} \left( \frac{H_{\phi a}}{r_e} + \frac{\partial H_{\phi a}}{\partial z} \right) = \frac{1}{\varepsilon_b} \left( \frac{H_{\phi b}}{r_e} + \frac{\partial H_{\phi b}}{\partial z} \right) \qquad (13a)$$

and

$$\left( \frac{E_{\phi a}}{r_e} + \frac{\partial E_{\phi a}}{\partial z} \right) = \left( \frac{E_{\phi b}}{r_e} + \frac{\partial E_{\phi b}}{\partial z} \right). \qquad (13b)$$

We now switch independent variables using equation (2). In the case of vertical polarization one derives from equation (10d)

$$n_a u_{Va} = n_b u_{Vb} \qquad (14a)$$

A5

while equation (13a) gives

$$\left(\frac{1}{n_a^2}\frac{\partial n_a}{\partial z} + \frac{1}{2n_a r_e}\right)u_{Va} + \frac{1}{n_a}\frac{\partial u_{Va}}{\partial z} = \left(\frac{1}{n_b^2}\frac{\partial n_b}{\partial z} + \frac{1}{2n_b r_e}\right)u_{Vb} + \frac{1}{n_b}\frac{\partial u_{Vb}}{\partial z}. \tag{14b}$$

Switching to modified refraction $m$, in using equation (7b) these equations become

$$m_a u_{Va} = m_b u_{Vb} \tag{15a}$$

and

$$\left(\frac{1}{m_b^2}\frac{\partial m_b}{\partial z} - \frac{1}{2m_b r_e}\right)u_{Vb} + \frac{1}{m_b}\frac{\partial u_{Vb}}{\partial z} = \left(\frac{1}{m_a^2}\frac{\partial m_a}{\partial z} - \frac{1}{2m_a r_e}\right)u_{Va} + \frac{1}{m_a}\frac{\partial u_{Va}}{\partial z}. \tag{15b}$$

For the case of horizontal polarization, use of equation (2b) and equations (10a) and (12) gives

$$u_{Ha} = u_{Hb} \qquad \text{and} \qquad \frac{\partial u_{Ha}}{\partial z} = \frac{\partial u_{Hb}}{\partial z}. \tag{16a, b}$$

For efficient numerical computation, the approach taken here treats the variable terrain in terms of staircase approximations using smooth earth formulae for the horizontal boundary conditions. The smooth earth boundary conditions are simplifications of the general boundary conditions for variable terrain. These conditions can be determined without approximations to the terrain, for the cases of vertical and horizontal polarization, in terms of directions normal and parallel to the terrain. Using a generalization of the earth flattening transformation that is applicable to the variable terrain, the general conditions can also be given in earth flattened coordinates $(x, z)$. For brevity these formulae are not included.

We now discuss the discontinuity at vertical interfaces, whether real (due to range dependent changes in refraction) or numerical (due to stair case approximations to terrain slopes.) Any parabolic equation requires two conditions in height and one condition in range to determine a unique solution. We have just derived the two height conditions at horizontal interfaces for each polarization case. When considering the condition at vertical interfaces, once an initial field has been specified, at each step in range the typical condition is continuity of field. That is to say that when a set of loss values has been computed at a particular range step, these values are used as initial data for taking the next range step. This condition can be replaced by other possible more desirable conditions. We use results from scalar acoustic problems to derive a conservation of energy condition for the vertical interface [9–12].

The basic concept is to introduce a new dependent variable obtained by scaling the old variable. The scale could be height-dependent. In order to properly implement an energy-conserving condition at a vertical interface we must derive an expression for the energy flux in the range direction. We begin with the complex Poynting vector $S$, which is generally taken to give the flow of energy in a propagating electromagnetic field. The vector is defined as [1]

$$S = \tfrac{1}{2}E \times H^* \tag{17}$$

where the asterisk denotes complex conjugate. The average intensity of energy flow is taken as the real part of the complex Poynting vector. For the case of vertical polarization

$$S = \tfrac{1}{2}((E_\theta H_\phi^*)e_r - (E_r H_\phi^*)e_\theta). \tag{18}$$

A6

The energy flux in the $\theta$ direction, denoted $S_\theta$, is

$$S_\theta = -\tfrac{1}{2}\,\mathrm{Re}(E_r H_\phi^*). \tag{19}$$

Using Maxwell's equations and equation (2) in equation (19) gives

$$S_\theta = \frac{1}{2\omega\varepsilon_0 r^2 \sin\theta}\,\mathrm{Im}\left(\frac{\partial u_V}{\partial\theta}u_V^*\right). \tag{20}$$

In using equation (4) to switch to earth flattened coordinates the energy flux is given by

$$S_x = \frac{1}{2\omega\varepsilon_0 r_e}\exp\left(\frac{-2z}{r_e}\right)\mathrm{cosec}\left(\frac{x}{r_e}\right)\mathrm{Im}\left(\frac{\partial u_V}{\partial x}u_V^*\right). \tag{21}$$

The condition for conservation of energy along a vertical interface thereby becomes

$$\mathrm{Im}\left(\frac{\partial u_{V_{tr}}}{\partial x}u_{V_{tr}}^*\right) = \mathrm{Im}\left(\frac{\partial u_{V_{in}}}{\partial x}u_{V_{in}}^*\right) \tag{22}$$

where we use the subscript 'in' here to denote the incident wave while 'tr' denotes the transmitted wave.

This type of nonlinear boundary condition is quite difficult to implement in practice, however an equivalent linear condition can be derived. By factoring equation (8a), and retaining the outgoing solution, one can derive

$$\frac{\partial u_V}{\partial x} = ik_0 Q_V u_V \tag{23a}$$

where

$$k_0 Q_V = \sqrt{\frac{\partial}{\partial z^2} + K_V^2}. \tag{23b}$$

Using equation (23) in equation (22) gives

$$\mathrm{Im}(i Q_{V_{tr}}|u_{V_{tr}}|^2) = \mathrm{Im}(i Q_{V_{in}}|u_{V_{in}}|^2) \tag{24a}$$

which will be satisfied if

$$Q_{V_{tr}}^{1/2}u_{V_{tr}} = Q_{V_{in}}^{1/2}u_{V_{in}}. \tag{24b}$$

One could in theory apply equation (24b) as the propagator for steps across vertical discontinuities. The simpler method of incorporating conservation conditions via a new dependent variable is derived by assuming negligible propagation angles. With this assumption, and those to follow, equations (8b) and (23b) yield the approximation $Q^{1/2} \approx (K_V^2/k_0^2)^{1/4} \approx \sqrt{m}$ so that the condition becomes

$$\sqrt{m_{tr}}u_{V_{tr}} = \sqrt{m_{in}}u_{V_{in}} \tag{25}$$

where $m$ is a modified index of refraction defined by equation (9). In deriving equation (25), one must assume that the terms involving $z$ derivatives of $m^{-1}$ are negligible. We obtain here merely a first-order correction for conserving energy. If one desired, one could implement

the full correction, given in equation (24b) at each range step where there is a vertical discontinuity of some type. This compounds the numerical process, however, and slows down the algorithm significantly. It has been demonstrated that the first-order correction is sufficient for many types of environments when considering acoustic propagation [9]. Tests underway also tend to support this conclusion for electromagnetic problems as well.

Equation (25) suggests the transformation of dependent variable to be

$$w_V = \sqrt{m}\,u_V \tag{26}$$

and continuity of field in $w$ will imply a first-order correction for conservation of energy in $u$. The case of horizontal polarization is analysed in a similar fashion leading to analogous results and a transformation identical to equation (25). For brevity, these results are omitted.

In using this transformation for conserving energy the elliptic equation that is solved is given as

$$\frac{\partial^2 w_i}{\partial x^2} + \sqrt{m}\frac{\partial^2}{\partial z^2}\left(\frac{w_i}{\sqrt{m}}\right) + K_i^2 w_i = 0 \tag{27}$$

where this equation has been derived by substituting equation (26) into equation (8a). In implementing the energy-conserving transformation one must now transform the interface conditions given in equations (15) and (16). For the case of vertical polarization conditions on $w_V$ become

$$\sqrt{m_a}\,w_{Va} = \sqrt{m_b}\,w_{Vb} \tag{28a}$$

and

$$\frac{1}{2}\left(\frac{1}{m_a^{5/2}}\frac{\partial m_a}{\partial z} - \frac{1}{r_e m_a^{3/2}}\right)w_{Va} + \frac{1}{m_a^{3/2}}\frac{\partial w_{Va}}{\partial z} = \frac{1}{2}\left(\frac{1}{m_b^{5/2}}\frac{\partial m_b}{\partial z} - \frac{1}{r_e m_b^{3/2}}\right)w_{Vb} + \frac{1}{m_b^{3/2}}\frac{\partial w_{Vb}}{\partial z}. \tag{28b}$$

The conditions on $w_H$ for the case of horizontal polarization become

$$\frac{1}{\sqrt{m_a}}w_{Ha} = \frac{1}{\sqrt{m_b}}w_{Hb} \tag{29a}$$

and

$$-\frac{1}{2m_a^{3/2}}\frac{\partial m_a}{\partial z}w_{Ha} + \frac{1}{\sqrt{m_a}}\frac{\partial w_{Ha}}{\partial z} = -\frac{1}{2m_b^{3/2}}\frac{\partial m_b}{\partial z}w_{Hb} + \frac{1}{\sqrt{m_b}}\frac{\partial w_{Hb}}{\partial z}. \tag{29b}$$

The preceding derivation has assumed that the complex part of $m$ is small compared to the real part. This is true over most of the frequency regime and terrain cover of interest.


## 4. Numerical implementation

Our goal is to solve the differential equation, equation (27),

$$\frac{\partial^2 w_i}{\partial x^2} + \sqrt{m}\frac{\partial^2}{\partial z^2}\left(\frac{w_i}{\sqrt{m}}\right) + K_i^2 w_i = 0$$

subject to homogeneous Dirichlet conditions at the boundaries, and the interface conditions in equation (28) for vertical polarization or equation (29) for horizontal polarization. The modified wavenumber, $K_i$, is defined in equation (8b). For convenience in upcoming notation, we drop the $i$ subscript in favour of the reader understanding that all results apply to both the vertical and horizontal polarization cases. This equation may be formally factored to give

$$\frac{\partial w}{\partial x} = ik_0 \sqrt{1 + Q} \, w \tag{30a}$$

where

$$k_0^2 Q = \sqrt{m} \frac{\partial^2}{\partial z^2} \frac{1}{\sqrt{m}} + K^2 - k_0^2 \tag{30b}$$

as the differential equation governing the outwardly propagating wave. The differences between this formulation and that in equation (23) is numerically motivated and will be discussed shortly. Removing the $\exp(ik_0x)$ from the solution $u$, equation (30a) becomes

$$\frac{\partial w}{\partial x} = ik_0 \left( -1 + \sqrt{1 + Q} \right) w. \tag{31}$$

One may formally integrate equation (31) to give

$$w(x + \Delta x, z) = \exp \left( ik_0 \Delta x \left( -1 + \sqrt{1 + Q} \right) \right) w(x, z). \tag{32}$$

Following the method of Collins we apply a Padé approximation [7]:

$$\exp \left( ik_0 \Delta x \left( -1 + \sqrt{1 + Q} \right) \right) \cong 1 + \sum_{l=1}^{np} \frac{a_{l,np} Q}{1 + b_{l,np} Q} \tag{33}$$

where the coefficients $a_{l,np}$ and $b_{l,np}$ are determined numerically using the approach in [11]. The method used in [11] converges faster using the formulation in equation (30) than that in equation (23). The number $np$ is the Padé number, or the number of terms used in the series approximation.

Substituting equation (33) into equation (32) one obtains the split-step Padé solution,

$$w(x + \Delta x, z) = w(x, z) + \sum_{l=1}^{np} \frac{a_{l,np} Q w(x, z)}{1 + b_{l,np} Q}. \tag{34}$$

The terms in the sum may be computed in parallel, which is what makes this technique so appealing. That is we compute

$$\psi_l(x, z) = \frac{a_{l,np} Q w(x, z)}{1 + b_{l,np} Q} \tag{35a}$$

in parallel and then calculate

$$w(x + \Delta x, z) = w(x, z) + \sum_{l=1}^{np} \psi_l(x, z). \tag{35b}$$

A9

Let us discretize the problem as follows. First we will use a simple linear transformation to invert the problem so that $z$ is measured positive down from the top of the atmosphere. For ease of notation we will still use the variable $z$ rather than defining a new variable, say $z'$. Then we define a grid with mesh sizes $dx$, and $dz$. Let

$$w_j^n = w(n\,dx, j\,dz) \tag{36a}$$

and

$$\psi_{l,j}^n = \psi_l(n\,dx, j\,dz) \tag{36b}$$

When discretizing the differential operator $Q$, equation (35a) becomes a tridiagonal linear system of which the $j$th equation is

$$R1_{l,j}\psi_{l,j-1}^n + R2_{l,j}\psi_{l,j}^n + R3_{l,j}\psi_{l,j+1}^n = S1_{l,j}w_{j-1}^n + S2_{l,j}w_j^n + S3_{l,j}w_{j+1}^n \tag{37}$$

where $R1$, $R2$, $R3$, $S1$, $S2$, and $S3$, are dependent upon $dz$ and medium properties through the function $K$ and $m$. Once this system is solved for $\psi_{l,j}^n$ one uses equation (35b) to compute the solution $w_j^{n+1}$ as

$$w_j^{n+1} = w_j^n + \sum_{l=1}^{np} \psi_{l,j}^n. \tag{38}$$

The numerical domain is terminated with homogeneous Dirichlet conditions on the field $w$. To avoid spurious reflections from the top of the atmosphere, an absorbing layer is introduced with complex wavenumber. Similarly, at the bottom of the earth layer, one increases conductivity so as to eliminate reflections. For most typical ground cover with non-zero conductivity the Earth acts as an absorbing layer naturally. Increasing conductivity near the bottom of the domain insures no reflections. As for implementing the interface conditions as given in equations (28) and (29) one uses the idea of virtual points [11]. Assume the atmosphere–terrain interface occurs between the $j$th and $(j+1)$th notch points. We place two virtual points $a'$ and $b'$ in between the two actual points, such that the point $a'(b')$ represents the continuation of the atmospheric (terrain) solution one notch point.

This technique is described fully in [10]. By requiring each $\psi_{l,j}^n$ to satisfy the linear interface conditions at the earth's surface, one automatically satisfies the interface requirement on the entire solution $w_j^n$. The discretized equations at the nodes on each side of the interface are

$$R1_{l,j}\psi_{l,j-1}^n + R2_{l,j}\psi_{l,j}^n + R3_{l,j}\psi_{l,a'}^n = S1_{l,j}w_{j-1}^n + S2_{l,j}w_j^n + S3_{l,j}w_{a'}^n \tag{39a}$$

and

$$R1_{l,j+1}\psi_{l,b'}^n + R2_{l,j+1}\psi_{l,j+1}^n + R3_{l,j+1}\psi_{l,j+2}^n = S1_{l,j+1}w_{b'}^n + S2_{l,j+1}w_{j+1}^n + S3_{l,j+1}w_{j+2}^n \tag{39b}$$

We approximate

$$w_a = \tfrac{1}{2}(w_j^n + w_{a'}^n) \qquad w_b = \tfrac{1}{2}(w_{j+1}^n + w_{b'}^n) \tag{40a, b}$$

$$\frac{\partial w_a}{\partial z} = \frac{w_{a'}^n - w_j^n}{dz} \qquad \text{and} \qquad \frac{\partial w_b}{\partial z} = \frac{w_{j+1}^n - w_{b'}^n}{dz} \tag{40c, d}$$

A10

at the interface, and substituting these expressions in equation (28) for vertical polarization or equation (29) for horizontal polarization allows one to solve for the virtual point solutions in terms of actual notch point solutions. For the case of vertical polarization, using equation (40) in equation (28) gives

$$A_1(w_j^n + w_{a'}^n) = A_2(w_{j+1}^n + w_{b'}^n) \tag{41a}$$

and

$$A_3(w_j^n + w_{a'}^n) + A_4(w_{a'}^n - w_j^n) = A_5(w_{j+1}^n + w_{b'}^n) + A_6(w_{j+1}^n - w_{b'}^n) \tag{41b}$$

where

$$A_1 = \sqrt{m_a} \qquad A_2 = \sqrt{m_b} \tag{41c, d}$$

$$A_3 = \frac{dz}{4}\left(\frac{1}{r_e m_a^{3/2}} + \frac{1}{m_a^{5/2}}\frac{\partial m_a}{\partial z}\right) \qquad A_4 = \frac{1}{m_a^{3/2}} \tag{41e, f}$$

$$A_5 = \frac{dz}{4}\left(\frac{1}{r_e m_b^{3/2}} + \frac{1}{m_b^{5/2}}\frac{\partial m_b}{\partial z}\right) \qquad \text{and} \qquad A_6 = \frac{1}{m_b^{3/2}}. \tag{41g, h}$$

Solving equations (41a) and (41b) for the virtual solutions gives

$$w_{a'}^n = \alpha_{11} w_j^n + \alpha_{12} w_{j+1}^n \tag{42a}$$

and

$$w_{b'}^n = \alpha_{21} w_j^n + \alpha_{22} w_{j+1}^n \tag{42b}$$

where

$$\alpha_{11} = (A_1(A_5 - A_6) + A_2(A_4 - A_3))/(A_1(A_6 - A_5) + A_2(A_3 + A_4)) \tag{42c}$$

$$\alpha_{12} = (2A_2 A_6)/(A_1(A_6 - A_5) + A_2(A_3 + A_4)) \tag{42d}$$

$$\alpha_{21} = (2A_1 A_4)/(A_1(A_6 - A_5) + A_2(A_3 + A_4)) \tag{42e}$$

and

$$\alpha_{22} = (A_1(A_5 + A_6) - A_2(A_3 + A_4))/(A_1(A_6 - A_5) + A_2(A_3 + A_4)). \tag{42f}$$

One may also repeat this procedure for each individual $\psi_{l,j}^n$, and since they each satisfy the same interface conditions one uses equation (42) exactly for virtual point solutions $\psi_{l,a'}^n$ and $\psi_{l,b'}^n$. The result is that at the interface equation (39) becomes

$$R1_{l,j}\psi_{l,j-1}^n + (R2_{l,j} + \alpha_{11}R3_{l,j})\psi_{l,j}^n + \alpha_{12}R3_{l,j}\psi_{l,j+1}^n$$
$$= S1_{l,j}w_{j-1}^n + (S2_{l,j} + \alpha_{11}S3_{l,j})w_j^n + \alpha_{12}S3_{l,j}w_{j+1}^n, \tag{43a}$$

and

$$\alpha_{21}R1_{l,j+1}\psi_{l,j}^n + (R2_{l,j+1} + \alpha_{22}R1_{l,j+1})\psi_{l,j+1}^n + R3_{l,j+1}\psi_{l,j+2}^n$$
$$= \alpha_{21}S1_{l,j+1}w_j^n + (S2_{l,j+1} + \alpha_{22}S1_{l,j+1})w_{j+1}^n + S3_{l,j+1}w_{j+2}^n. \tag{43b}$$

A similar analysis in the horizontal polarization case yields very similar results in terms of equation (43), with differences in the definitions of the $\alpha_{ij}$ coefficients. Using equation (40) in equation (29) gives the equations

$$\bar{A}_1(w_j^n + w_{a'}^n) = \bar{A}_2(w_{j+1}^n + w_{b'}^n) \tag{44a}$$

and

$$\bar{A}_3(w_j^n + w_{a'}^n) + \bar{A}_1(w_{a'}^n - w_j^n) = \bar{A}_4(w_{j+1}^n + w_{b'}^n) + \bar{A}_2(w_{j+1}^n - w_{b'}^n) \tag{44b}$$

where now

$$\bar{A}_1 = \frac{1}{\sqrt{m_a}} \qquad \bar{A}_2 = \frac{1}{\sqrt{m_b}} \tag{44c, d}$$

$$\bar{A}_3 = -\frac{1}{4m_a^{3/2}}\frac{\partial m_a}{\partial z} \qquad \text{and} \qquad \bar{A}_4 = -\frac{1}{4m_b^{3/2}}\frac{\partial m_b}{\partial z}. \tag{44e, f}$$

Solving equations (44a) and (44b) for $w_{a'}^n$ and $w_{b'}^n$ yields

$$w_{a'}^n = \bar{\alpha}_{11}w_j^n + \bar{\alpha}_{12}w_{j+1}^n \tag{45a}$$

and

$$w_{b'}^n = \bar{\alpha}_{21}w_j^n + \bar{\alpha}_{22}w_{j+1}^n \tag{45b}$$

where

$$\bar{\alpha}_{11} = \bar{\alpha}_{22} = (\bar{A}_1\bar{A}_4 - \bar{A}_2\bar{A}_3)/(2\bar{A}_1\bar{A}_2 + \bar{A}_2\bar{A}_3 - \bar{A}_1\bar{A}_4) \tag{45c}$$

$$\bar{\alpha}_{12} = (2\bar{A}_2^2)/(2\bar{A}_1\bar{A}_2 + \bar{A}_2\bar{A}_3 - \bar{A}_1\bar{A}_4) \tag{45d}$$

and

$$\bar{\alpha}_{21} = (2\bar{A}_1^2)/(2\bar{A}_1\bar{A}_2 + \bar{A}_2\bar{A}_3 - \bar{A}_1\bar{A}_4). \tag{45e}$$

The final implementation is exactly that in equation (43) with $\alpha_{ij}$ being replaced by $\bar{\alpha}_{ij}$.

Therefore the numerical implementation of the terrain interface is a simple modification of the algorithm at the $j$th and $(j + 1)$th nodes. The code SSP is currently undergoing testing. The next section discusses preliminary testing and evaluation of SSP including the atmosphere–terrain interface implementation.

## 5. Numerical examples

The numerical code SSP is currently being tested. The results presented in this paper do not utilize the advantage of parallel processing. Preliminary solutions were calculated on PCs simply to test the code and demonstrate certain aspects of this method. The final program will be run on a parallel machine. References [8–10] suggest run time speeds 100 times faster than conventional methods.

Since the implementation of interface matching conditions is an integral part of the program, examination of the numerical methods used there is critical. While some acoustic propagation models do incorporate horizontal interfaces many more do not. It seems that the discontinuity in the acoustic case is slight as compared to the EM case. So slight as to permit one to smooth out discontinuities or simply ignore them altogether. This is certainly not the case for electromagnetic propagation. A series of tests, too comprehensive to present here, have examined this aspect of the problem. By altering acoustic parameters so as to have a discontinuity of order similar to the EM case, the results show that one must also incorporate the acoustic matching conditions to have accurate solutions.

The simplest analytical model to test the method is the Lloyds mirror problem, in which the medium is taken as homogeneous, with homogeneous Dirichlet conditions at the top and bottom of the domain. The source frequency is taken as 4.99 MHz, with $dr = 2$ m, and $dz = 0.5$ m. The source and receiver height are both taken to be 75 m, and the entire thickness of the domain is 200 m. Figure 1(a) shows a comparison of the propagation losses as computed by the program SSP (full curve) and the program EFEPE (dotted). The code EFEPE is the original acoustic code and was benchmarked against a normal mode program showing excellent agreement [7]. As one can see there is virtually no difference in solutions. We were satisfied that the EM adaptation was coded correctly. We next considered the interface modelling. We are currently looking into benchmark models for EM propagation so as to fully test the numerical implementation of the interface matching conditions. However, there are existing acoustic benchmark models available immediately. We are able to implement acoustic boundary conditions, similar to our electromagnetic conditions, in the code and compare them to results that were benchmarked against normal mode solutions. The model we choose is called Case 3b from the NORDA Parabolic Equation Workshop [13]. It is basically one homogeneous medium overlying a different homogeneous medium with absorption. The density discontinuity at the ocean–sea floor interface is very similar to the light speed discontinuity in the EM problem at the atmosphere–terrain interface. While the interface conditions for the acoustic model are not as complicated as the EM problem, the numerical implementation using virtual points is identical.

Having implemented the interface conditions in the acoustic code, figure 1(b) compares the results from SSP (full) and the original acoustic program EFEPE (dotted,) which was benchmarked against a normal mode solution. The output from EFEPE was in excellent agreement with the normal mode solution except at null locations, specifically the one near 7 km. While there are subtle differences in losses, they are at most 1 dB, and the curves generally agree quite well. Work is currently underway to test the EM interface conditions.

The remaining figures demonstrate the method's ability to greatly increase range step size. We will use the Lloyds mirror example to illustrate. Using the EFEPE result in figure 1(a) as a benchmark we have calculated the solution using the code SSP with $np = 4$ and $dr = 50$ m. Figure 2(a) shows the results with fair agreement that decays as range increases. When increasing $np$ to 8, as in figure 2(b), excellent accuracy is obtained. For parallel computations this could mean very little extra run time achieving much better accuracy. When the range step is increased to 100 m, as in figure 3(a), the accuracy is still maintained for $np = 8$. When the range step is increased to 200 m, the accuracy begins to degrade. Finally, when increasing $np$ to 10, shown in figure 4, accuracy, while still not perfect, is increased greatly.

In theory, one can take very large range steps when using this method. One need only take $np$ large enough so that the Padé approximation gets arbitrarily accurate. However, the limiting factor will be terrain and atmospheric conditions. Taking range steps too large could result in 'stepping over mountains'. As is typical with parabolic approximation methods,

A13
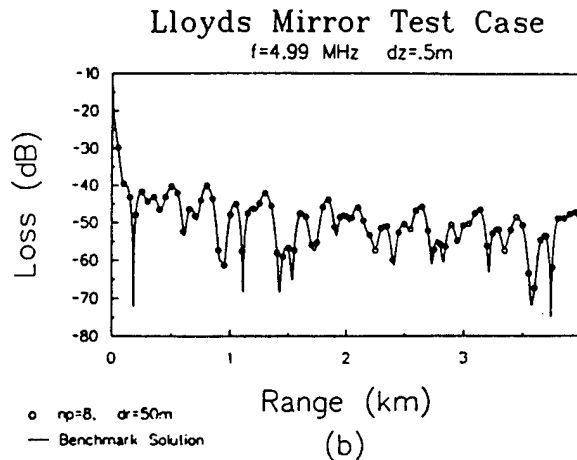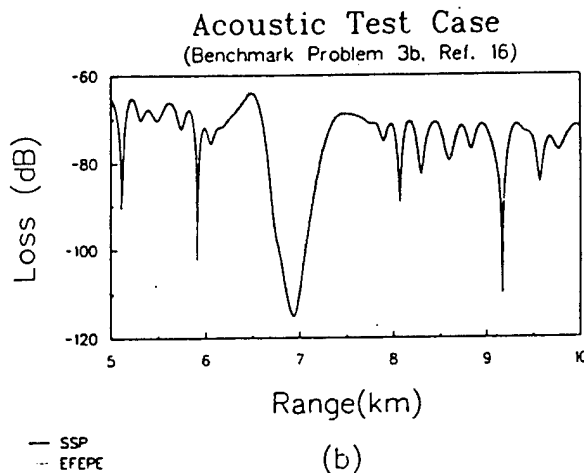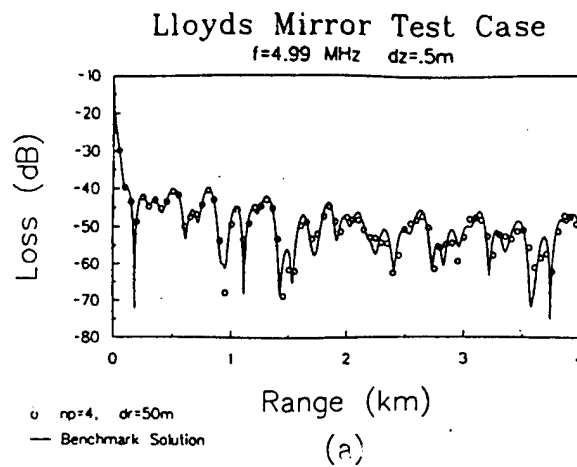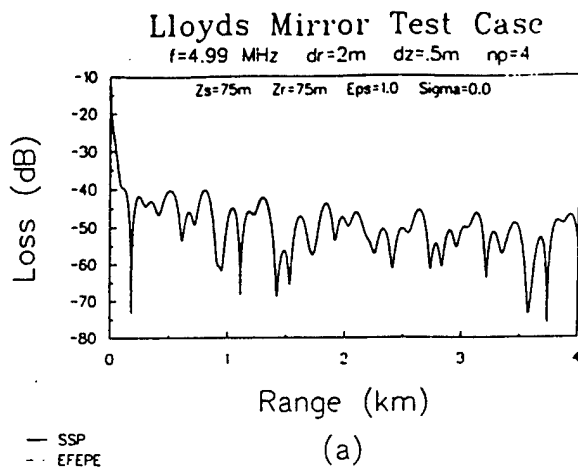
**Figure 1.** (a) The Lloyds mirror test problem. Source and receiver height are 75 m, and source frequency is 4.99 MHz. Intensity loss in dB is plotted against range in km. SSP (full curve) and EFEPE (dotted curve) show excellent agreement. (b) Acoustic benchmark Case 3b in [13]: SSP (full curve) and EFEPE (dotted curve) show excellent agreement.

**Figure 2.** Lloyds mirror test problem: comparison of SSP with benchmark solution for (a) $np = 4$ and $dr = 50$ m, and (b) $np = 8$, and $dr = 50$ m.

the range-dependent problem is sectored into range-independent slabs. Discretization of a continuous medium results in staircase effects. These effects are minimized by taking smaller range steps. Therefore there is still a lot of work to be done in the delicate matter of trading off time ($dr$ and $np$ as large as possible) and accuracy ($dr$ small enough to capture the true physical properties of the medium). Sensitivity testing and benchmarking are crucial aspects of this problem and current efforts are being placed on these areas.

## 6. Summary

Scalar Helmholtz equations have been derived directly from Maxwell's equations for the cases of vertical and horizontal polarization. The primary assumption necessary for such a reduction is that the medium is approximately symmetric in one spatial direction. Factorization of these equations yield parabolic equations which are then symbolically

## Lloyds Mirror Test Case
### f=4.99 MHz  dz=.5m



o  np=8,  dr=100m
— Benchmark Solution

(a)

## Lloyds Mirror Test Case
### f=4.99 MHz  dz=.5m



o  np=8,  dr=200m
— Benchmark Solution

(b)

## Lloyds Mirror Test Case
### f=4.99 MHz  dz=.5m



o  np=10,  dr=200m
— Benchmark Solution
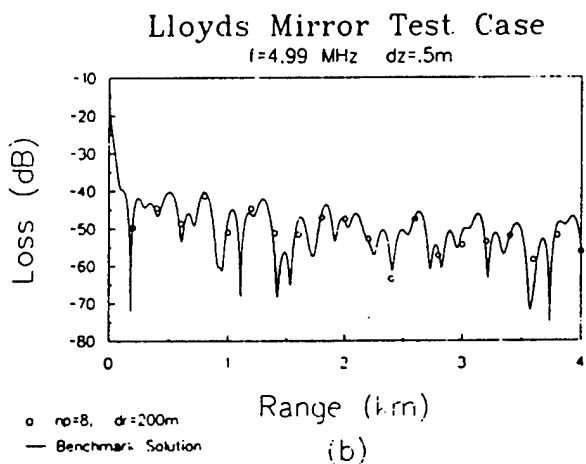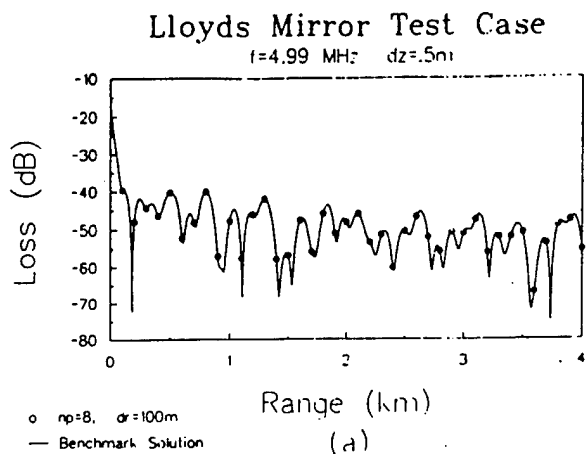
**Figure 3.** Lloyds mirror test problem: comparison of SSP with benchmark solution for (a) $np = 8$ and $dr = 100$ m, and (b) $np = 8$, and $dr = 200$ m.
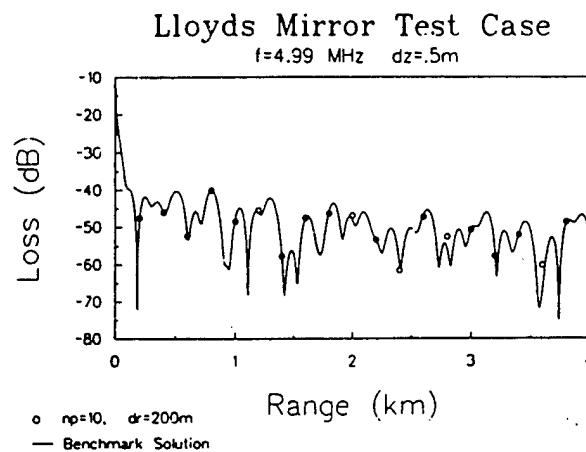
**Figure 4.** Lloyds mirror test problem: comparison of SSP with benchmark solution for $np = 10$ and $dr = 200$ m.

solved in the range direction. What one obtains is a symbolic expression for the range-stepping macroscopic operator. Rather than discretize the microscopic operator, a Padé series approximation is used for the macroscopic operator. In theory this allows very large range steps. Step size is still ultimately determined by medium characteristics. However there are numerical advantages over typical finite difference methods, the main being the suitability of the method to be parallelized for multi-processor computers.

Interface conditions have been fully developed for linking the atmosphere to the ground. Methods for conserving energy at vertical interfaces has also been discussed, with the result that to first order, a simple transformation of dependent variable allows for implementation. This will provide corrections to sloping terrain errors as well as range-dependent refractive effects. The numerical implementation of the split-step Padé solution and interface conditions has also been presented. Several benchmark calculations and interface modelling comparisons were also presented. A full description of the code SSP is contained in technical reports available from the authors upon request. The user's manual includes program flow charts, input descriptions and output options. Also described in this report is a post processing graphics program called GRAPH. This program produces contour graphs for visual display only.

A15

## Acknowledgments

## References

[1] Stratton J A 1941 *Electromagnetic Theory* (New York: McGraw-Hill)

[2] Tappert F D 1977 The parabolic approximation method *Wave Propagation and Underwater Acoustics (Lecture Notes in Physics 70)* ed Joseph B Keller and John S Papadakis (New York: Springer) pp 224–87

[3] Lee D, Botseas G and Papdakis J 1981 Finite difference solutions to the parabolic wave equations *J. Acoust. Soc. Am.* 70 795–800

[4] Hardin R H and Tappert F D 1973 Application of the split-step Fourier method to the numerical solution of nonlinear and variable coefficient wave equations *SIAM Rev.* 15 423

[5] Ko H W, Sari J W and Skura J P 1983 Anomalous microwave propagation through atmospheric ducts *Johns Hopkins APL Tech. Dig.* 4 12–26

[6] Lee D and Saied F 1990 A fourth-order difference scheme to improve the computational speed of wide angle propagation *Computational Acoustics* vol 1, ed D Lee, A Cakmak and R Vichnevetsky (New York: North-Holland) pp 27–35

[7] Collins M D 1993 A split-step Padé solution for the parabolic equation method *J. Acoust. Soc. Am.* 93 1736–42

[8] Collins M D 1993 The adiabatic mode parabolic equation *J. Acoust. Soc. Am.* 94 2269–78

[9] Collins M D 1991 A higher-order energy conserving parabolic equation for range-dependent ocean depth, sound speed, and density *J. Acoust. Soc. Am.* 89 1068–75

[10] Collins M D 1993 An energy-conserving parabolic equation for elastic media *J. Acoust. Soc. Am.* 94 975–82

[11] Collins M D 1989 A higher-order parabolic equation for wave propagation in an ocean overlying an elastic bottom *J. Acoust. Soc. Am.* 86 1459–64

[12] Collins M D 1992 A two-way parabolic equations for acoustic backscatter in the ocean *J. Acoust. Soc. Am.* 91 1357–68

[13] Davis J A, White D and Cavanagh R C 1982 NORDA Parabolic Equation Workshop *NORDA Technical Note* *(September)* 143

# Appendix B
# Absorbing Layer Validation

# Absorbing Layers

A major complication in the solution of propagation problems in physically infinite media is the attenuation of fictitious reflections from computational boundaries necessary to terminate the calculation. For full elliptic or hyperbolic problems the boundaries are not only the top or bottom of the domain but the right-hand edge. For a parabolic problem one need only worry about the top and bottom edges There are two approaches to solving such problems. The first technique is to use an impedance-type boundary condition at the computational edge. The second technique places an absorbing layer at the region in question. This layer has the property that the index of refraction has an imaginary component that varies with height. The absorbing potential (the imaginary piece) must vary in such a way as to eliminate reflections. The function has a maximum at the end of the absorbing layer (in our case near the top of the domain) and decreases exponentially as the distance from the boundary increases. I have obtained the following information from Dr. Steven Wales, at N.R.L., and I (he) has no explanation as to why it works but after years of experience this is what he and NRL came up with. The imaginary part of the index of refraction is taken as

$$v_0 \exp\left(\frac{-(z-z_B)^2}{(16\lambda)^2}\right)$$

where $v_0$ is taken to be .10 (in mks system)., and $\lambda$ is source wavelength. In terms of the reference wave number $k_0$, the function is

$$v_0 \exp\left(-9.8946468 \times 10^{-5} k_0^2 (z-z_B)^2\right)$$

Dr. Wales had suggested that for most frequencies of interest the width of the absorbing layer should be about 1/3 the thickness of the actual medium, however, he also mentioned that at the lower frequencies the width had to be greater. I began testing the layer by picking various width factors. After several test runs I have determined appropriate width factors for frequencies of 1, 3, 4, 5, 10, 20, and 25 MHz. It seems that for frequencies above 25 MHz, the choice of a width factor = 1/3 is in fact good. However, for the lower frequencies several values had to be selected. The results are summarized in the following table.

| Frequency (MHz) | Wave number $(k_0)$ | Width Factor |
|---|---|---|
| 1 | .020958 | 15 |
| 3 | .062874 | 6 |
| 4 | .083832 | 4 |
| 5 | .010479 | 2 |
| 10 | .20958 | 1 |
| 20 | .41916 | .56 |
| 25 | .52396 | 1/3 |

By width factor, I mean the amount of the requested physical domain that is extended. If HMAX1 is 750, and the width factor is 1/3 then the absorbing layer is computed as 250 m wide. If HMAX1 is 1000m, and the width factor is 13, then the absorbing layer is taken to be 13,000m. The following pages show comparisons of the code SSP with the analytica solution for an infinite homogeneous half space Dirichlet problem . The solution to the spherically symmetric wave equation is

$$u = \frac{1}{\rho}\exp(i k_0 \rho)$$

where $\rho$ is the distance from the source to the receiver.

Ignoring curvature effects, let a cylindrical coordinate system be placed so that . source is positioned on the $z$-axis at $(r,z_s)$. If the earth (at $z = 0$,) is such that $u = 0$ there one may use the method of images to determine that

$$u = \frac{1}{\rho_1}\exp(i k_0 \rho_1) - \frac{1}{\rho_2}\exp(i k_0 \rho_2),$$

where

$$\rho_1 = \sqrt{r^2 + (z-z_s)^2},$$

and

$$\rho_2 = \sqrt{r^2 + (z+z_s)^2}.$$

Figure 1-7 show a comparison of SSP and the analytical solution for frequencies of 1, 3, 4, 5, 10, 20, and 25 MHz. In each case there are three figures ( i.e. Fig (1a), (1b) and (1c) ), Figure #(a), shows the entire interval $0 < r < 50$ km, while Fig. #b, and #c show blow ups of the range intervals $0 < r < 2$ km and $48 < r < 50$ km respectively. Clearly there is excellent agreement. The source and receivers are positioned 250 m above the surface. I choose the medium to be 2000 m high. There are some phase errors early on, but I cannot be sure if the errors are due to the absorbing layer or the inherent problems that PE's have in the near-field. In either case the phase errors disappear soon afterwards. For a source frequency of 1 MHz, as seen in Fig (1c), there are differences of at most O(.01) dB. This is also true for $f = 3$ MHz (Fig. (2c)) and $f = 4$ MHz (Fig. (3c)). For source frequencies of 5, 10 and 20 MHz, the differences are even less than the preceding cases. These frequencies correspond to acoustic frequencies of approximately 25, 50, and 100 Hz. This was the frequency range of interest, I believe, to NRL and Steven Wales. For higher frequencies, the agreement begins to decay slightly as seen in Fig. (7c).

To check the programs interpolation of layer widths, I ran test cases for frequencies of 2, 3.5, 4.5, 7.5, 15, and 22.5 MHz. These results are shown in Fig. 8 - 14, with similar range intervals as in the first 7 graphs. The results show excellent agreement at the longer ranges with dB differences typically of the order .01. In some cases there are differences of up to .15 dB, but that is still quite excellent.

Figure 14 shows results for a source frequency of 50 MHz. This is the case where I saw the greatest difference. Clearly, there should be some modification of the amplitude and half-width of the Gaussian absorbing potential as frequency is increased. However, .15 dB is rather a small difference at 25 km which is more than 4000 wavelengths. For future work, I suggest that someone does look into modification of the absorbing potential for higher frequencies.

I also ran a few cases with different source and receiver locations for long ranges. Figure 15 show results for a source frequency of 6.2 MHz. The source is located at 182 m above the surface and the receiver is 262 m high. The maximum height (HMAX1) is 3000 m. As seen in Fig (15c), the solution begins to decay near $r = 100$ km. It is clear that while the differences are less than 1 dB, the oscillations are increasing. The differences are resolved by raising HMAX1 to 5000 m, as in Fig (15d), and errors are now again between .01 and .1 dB. Figure 16 is a situation where the source frequency is 72.1 MHz and source height is 151 m. The receiver is located at 82 m above the surface and HMAX1 = 2000 m. While the maximum range is 50 KM not 100 km as in the previous example, the number of

wavelengths is approximately 12,500. This is a very large problem. As seen in Fig (16c), there is again excellent agreement between the analytic and computed solutions.

I ran these odd number cases just to make sure I wasn't getting any funny results b placing the source and receiver at 250 m which was at a depth node (harmonically speakin; since the medium was 2000 m wide. Well, I now trust this aspect of the program. The ne work is to get to the Beam program.

Absorbing Layer Comparison (f = 1 MHz)

Loss (dB)

Range (km)

$z_s = z_R = 250$

$HMAXA = 2000$

( 1a )

# Absorbing Layer Comparison (f = 1 MHz)

Loss (dB) vs Range (km)

Absorbing Layer Comparison (f = 1 MHz)

Range (km)

Loss (dB)

True Soln

Comptd

(16)

B7

# Absorbing Layer Comparison (f = 3 MHz)



Loss (dB) vs Range (km)

$Z_s = Z_R = 250m$

Absorbing Layer Comparison (f = 3 MHz)

Range (km)

Loss (dB)

(2b)

Absorbing Layer Comparison (f = 3 MHz)

Absorbing Layer Comparison (f = 4 MHz)

Loss (dB)

Range (km)

$(3a)$

$z_s = z_R = 250m$

$H_{MAX1} = 2000 m$

B11

Absorbing Layer Comparison (f = 4 MHz)

Absorbing Layer Comparison (f = 4 MHz)

Loss (dB)

Range (km)

True Sln

Computed

(3c)

B13

# Absorbing Layer Comparison (f = 5 MHz)

Loss (dB)

-20   -40   -60   -80   -100   -120

Range (km)

0   10   20   30   40   50

↑ 833 wavelengths

(¹|₁)

$Z_s = Z_R = 250$ m

# Absorbing Layer Comparison (f = 5 MHz)



Range (km)

Loss (dB)

(4b)

Absorbing Layer Comparison (f = 5 MHz)

Loss (dB)

Range (km)

Absorbing Layer Comparison (f = 10 MHz)

Loss (dB)

Range (km)

$(S_q)$

↑ 1666 Wavelengths

$Z_S = Z_R = 250\,m$

$H_{MAX1} = 2000\,m$

B17

# Absorbing Layer Comparison (f = 10 MHz)

True Solution

Current

Range (km)

Loss (dB)

**Absorbing Layer Comparison (f = 10 MHz)**

Range (km)

Loss (dB)

(5ᵈ)

B19

Absorbong Layer Comparison (f = 20 MHz)

Loss (dB)

Range (km)

3333 wavelengths

$Z_s = Z_R = 250 m$

$W_{max} = 3000 m$

Absorbong Layer Comparison (f = 20 MHz)

Range (km)

Loss (dB)

(b)

Absorbong Layer Comparison (f = 20 MHz)

# Absorbing Layer Comparison (f = 25 MHz)

Range (km)

Loss (dB)

$Z_s = Z_a = 250m$

$Hmax\lambda = 2000m$

4165 wavelengths

(7a)

**Absorbing Layer Comparison (f = 25 MHz)**

Loss (dB) vs Range (km)

# Absorbing Layer Comparison (f = 25 MHz)



MAX DIFF
is $\frac{1}{20}$ dB

Not Bad

True Solution

Computed

.05 dB

**Range (km)**

**Loss (dB)**

(7c)

B25

Interpolation Check (f = 2 MHz)

Loss (dB)

Range (km)

Interpolation Check (f = 2 MHz)

Loss (dB)

Range (km)

(8b)

B27

Interpolation Check (f = 2 MHz)

Range (km)

Loss (dB)

Compile Solution

true Soln

Interpolation Check (f = 3.5 MHz)

Loss (dB)

Range (km)

(9a)

β29
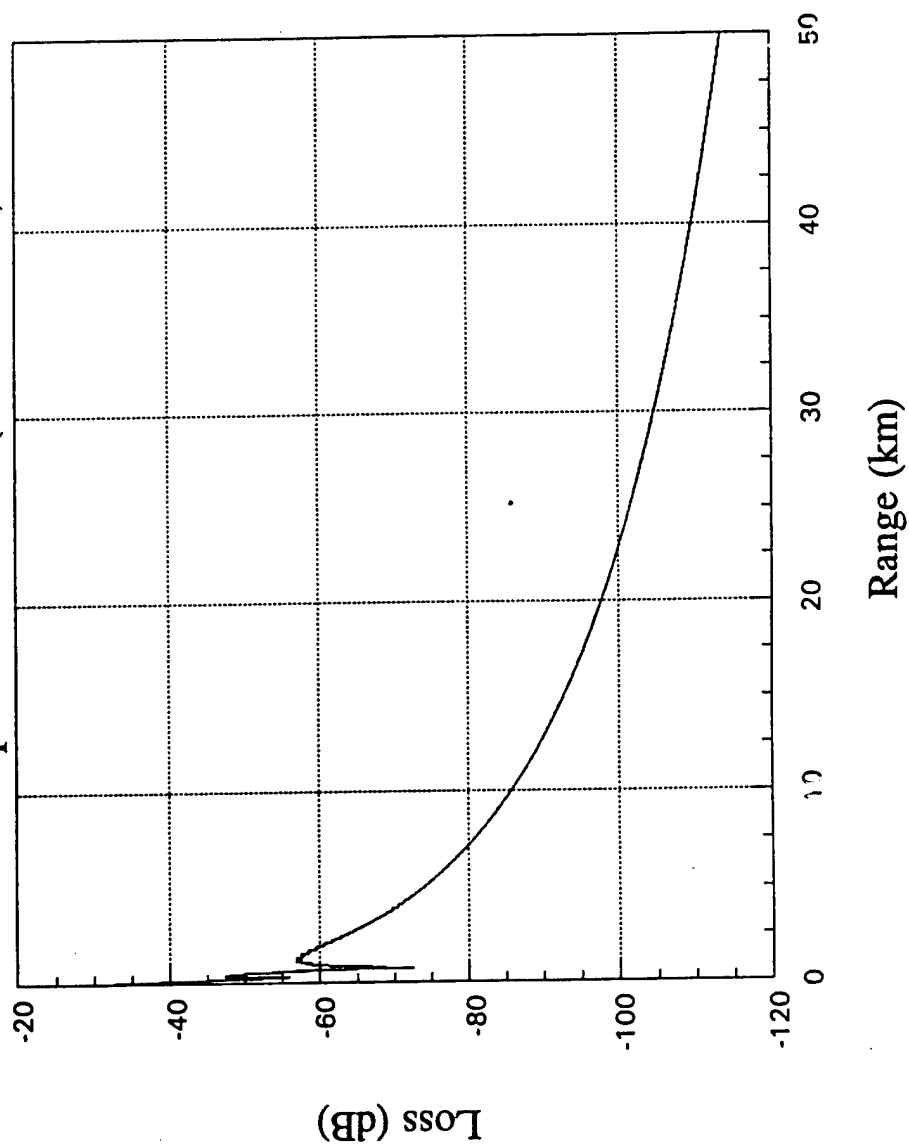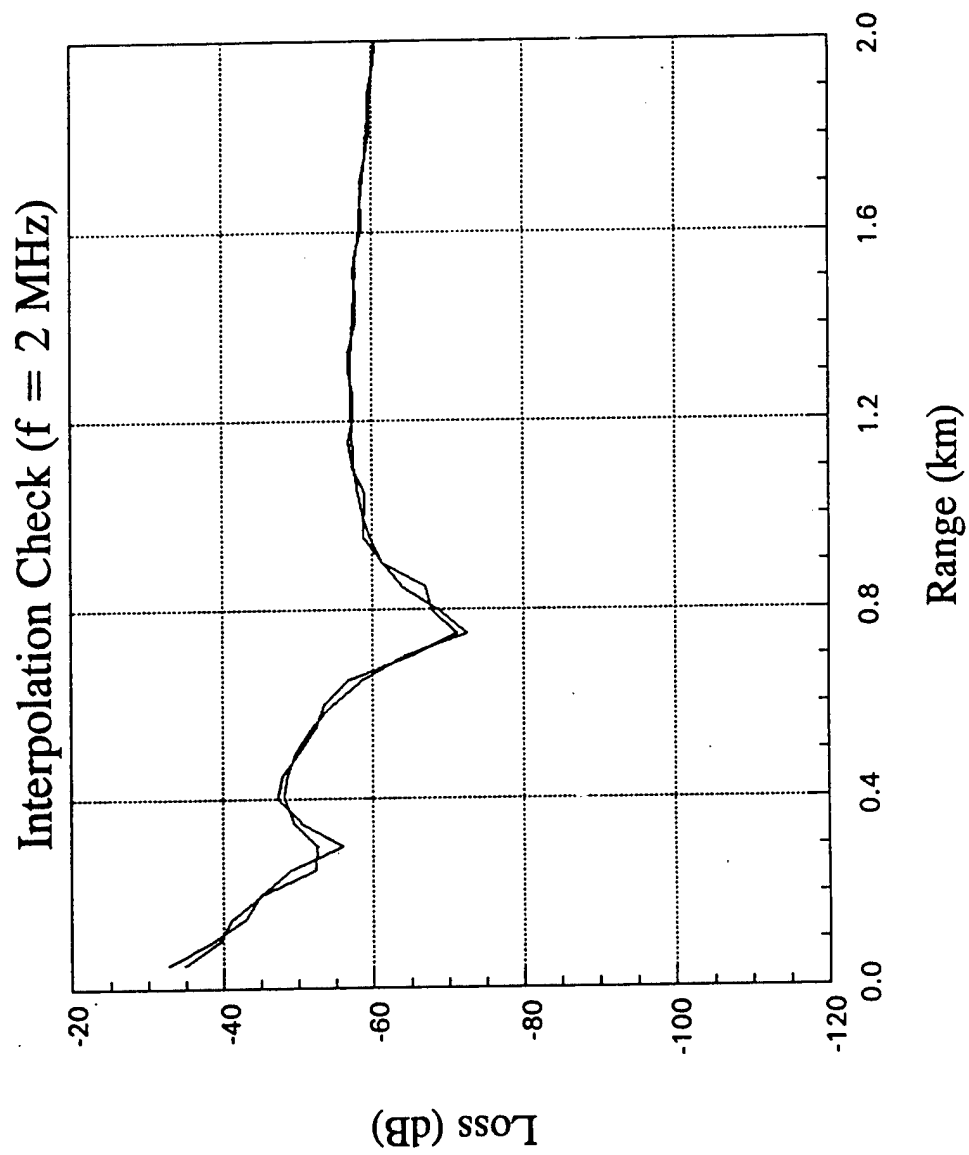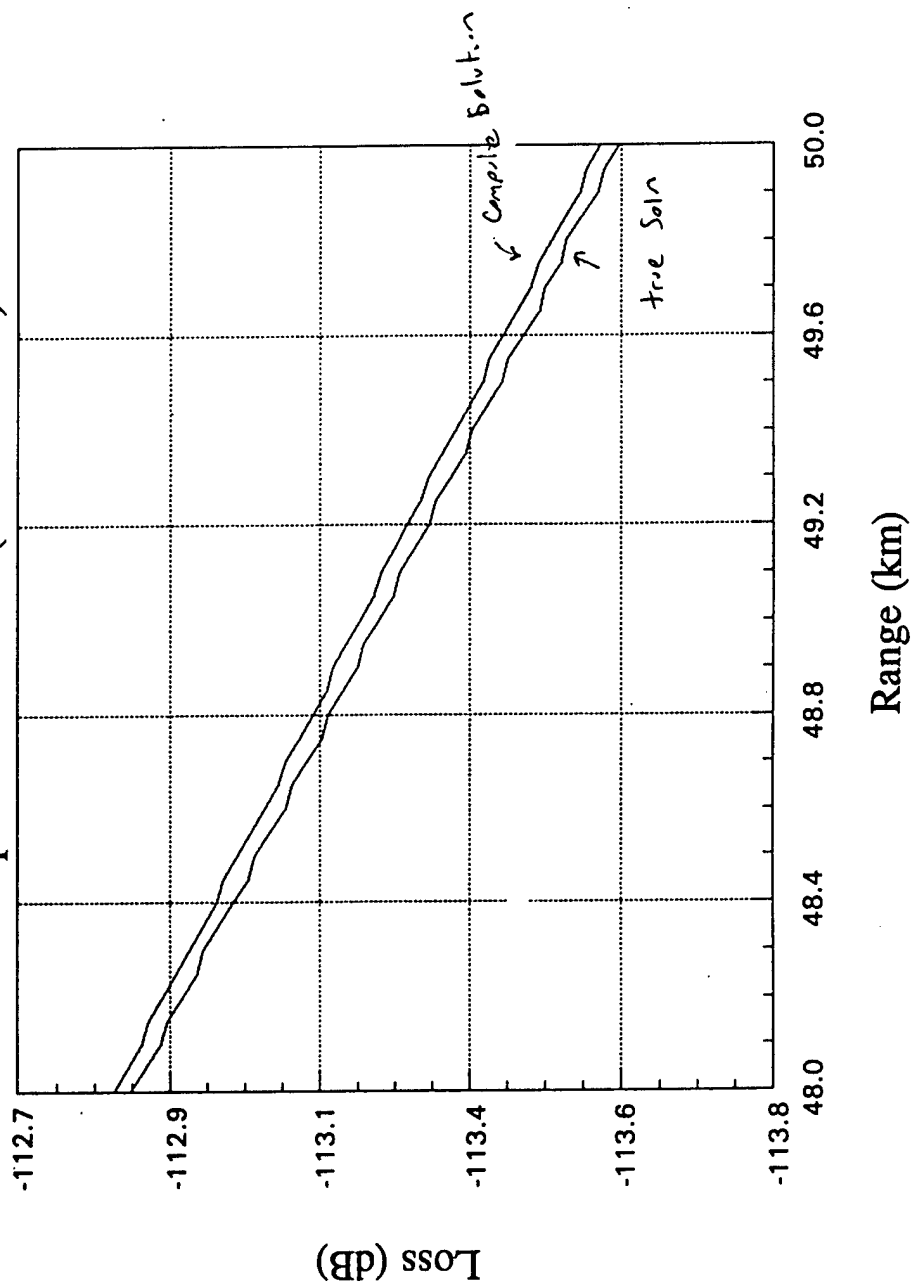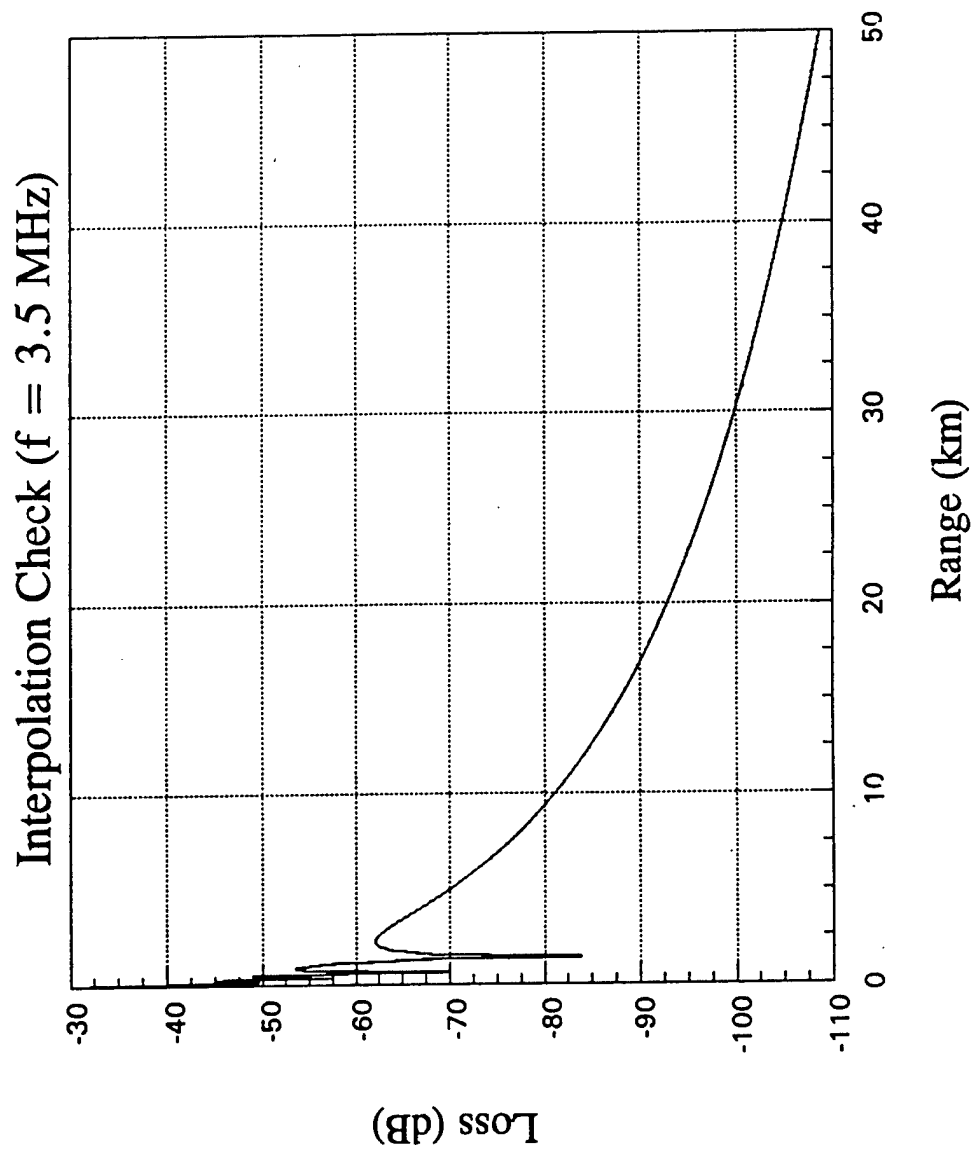
Interpolation Check (f = 3.5 MHz)

Interpolation Check (f = 3.5 MHz)

Loss (dB)

Range (km)

Corrupted

true soln

(9c)

Interpolation Check (f = 4.5 MHz)

Loss (dB)

Range (km)

Interpolation Check (f = 4.5 MHz)

Range (km)

Loss (dB)

(1ᵇ)

B33

# Interpolation Check (f = 4.5 MHz)



Plot of Loss (dB) versus Range (km). Vertical axis "Loss (dB)" ranges from -105.8 to -106.6. Horizontal axis "Range (km)" ranges from 48.0 to 50.0. Two curves labeled "Computed" and "True sol~".

Interpolation Check (f = 7.5 MHz)

Loss (dB)

Range (km)

(11a)

B35

Interpolation Check (f = 7.5 MHz)

Range (km)

Loss (dB)

(11b)

Interpolation Check (f = 7.5 MHz)

Loss (dB)

Range (km)

True

Lmp.hd

(11c)

# Interpolation Check (f = 15 MHz)

Range (km)

(17a)

Loss (dB)

B38

Interpolation Check (f = 15 MHz)

Loss (dB)

Range (km)

(12b)

B39

# Interpolation Check (f = 15 MHz)

Loss (dB) vs Range (km)

A plot with Y-axis "Loss (dB)" ranging from -95.3 to -96.3, and X-axis "Range (km)" ranging from 48.0 to 50.0. A nearly linear curve decreases from about -95.6 at 48.0 km to about -96.3 at 50.0 km.

(J2c)

Interpolation Check (f = 22.5 MHz)

Loss (dB)

Range (km)

(13a)

B41

wavelengths is approximately 12,500. This is a very large problem. As seen in Fig (16c), there is again excellent agreement between the analytic and computed solutions.

I ran these odd number cases just to make sure I wasn't getting any funny results b placing the source and receiver at 250 m which was at a depth node (harmonically speakin since the medium was 2000 m wide. Well, I now trust this aspect of the program. The ne work is to get to the Beam program.

Interpolation Check (f = 22.5 MHz)

Range (km)

Loss (dB)

(36)

B42

Interpolation Check (f = 22.5 MHz)

Loss (dB)

Range (km)

(13c)

343

Interpolation Check (f = 50 MHz)

Loss (dB)

Range (km)

(14a)

Interpolation Check (f = 50 MHz)

Loss (dB)

Range (km)

( 145 )

B45

## Interpolation Check (f = 50 MHz)

Loss (dB)

Range (km)

'0.13 dB'

(14c)

# Freq. = 6.2 MHz  (Interpolation Check)
### HMAX1 = 3000m



Loss (dB) vs Range (km)

↑ ~ 2000λ

( 154 )

$Z_s = 182m$

$Z_R = 262m$

$dr = 25m$

$HMAX1 = 3000m$

B47

# Freq. = 6.2 MHz (Interpolation Check)
$Hmax1 = 3000m$



Loss (dB) vs Range (km)

(15b)

Freq. = 6.2 MHz  (Interpolation Check)

HMAX1 = 3000 m

Loss (dB)

Range (km)

exact

computed

(15c)
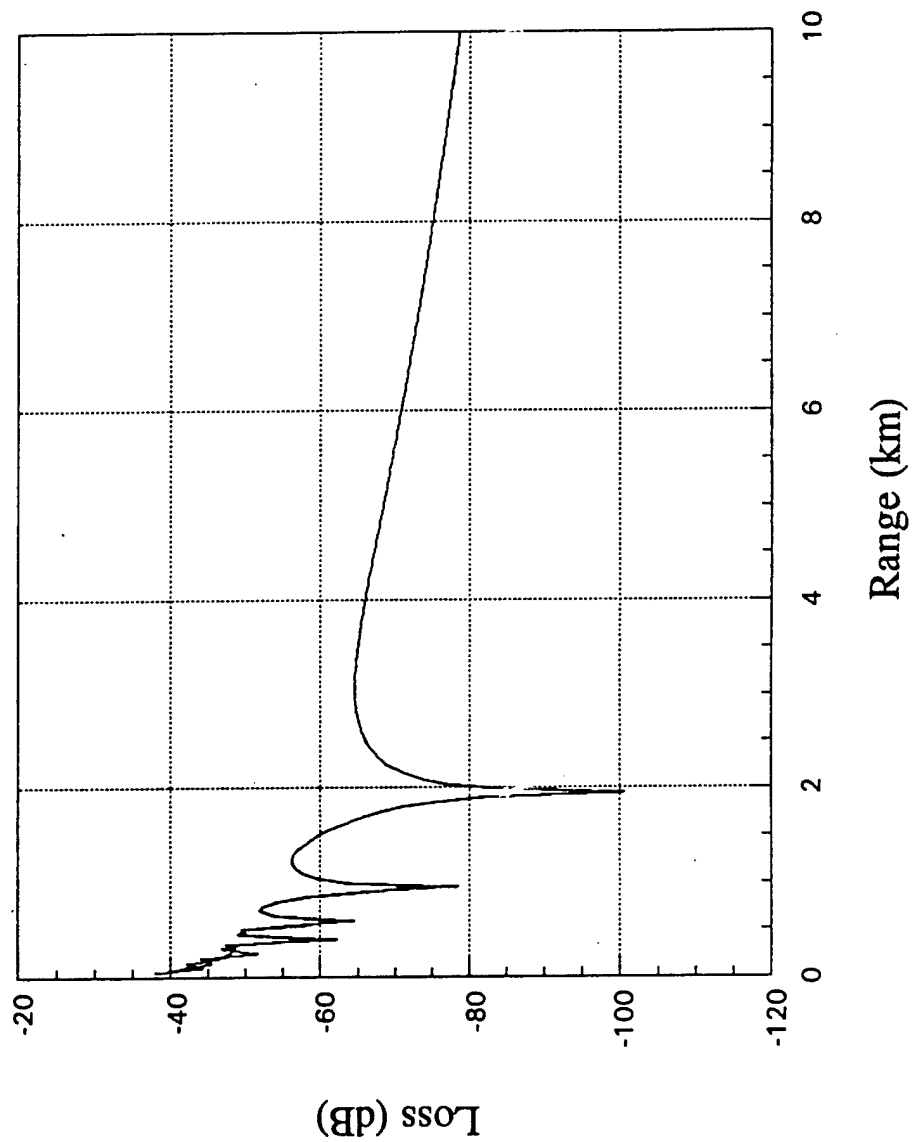
Blow Up

Note scale change
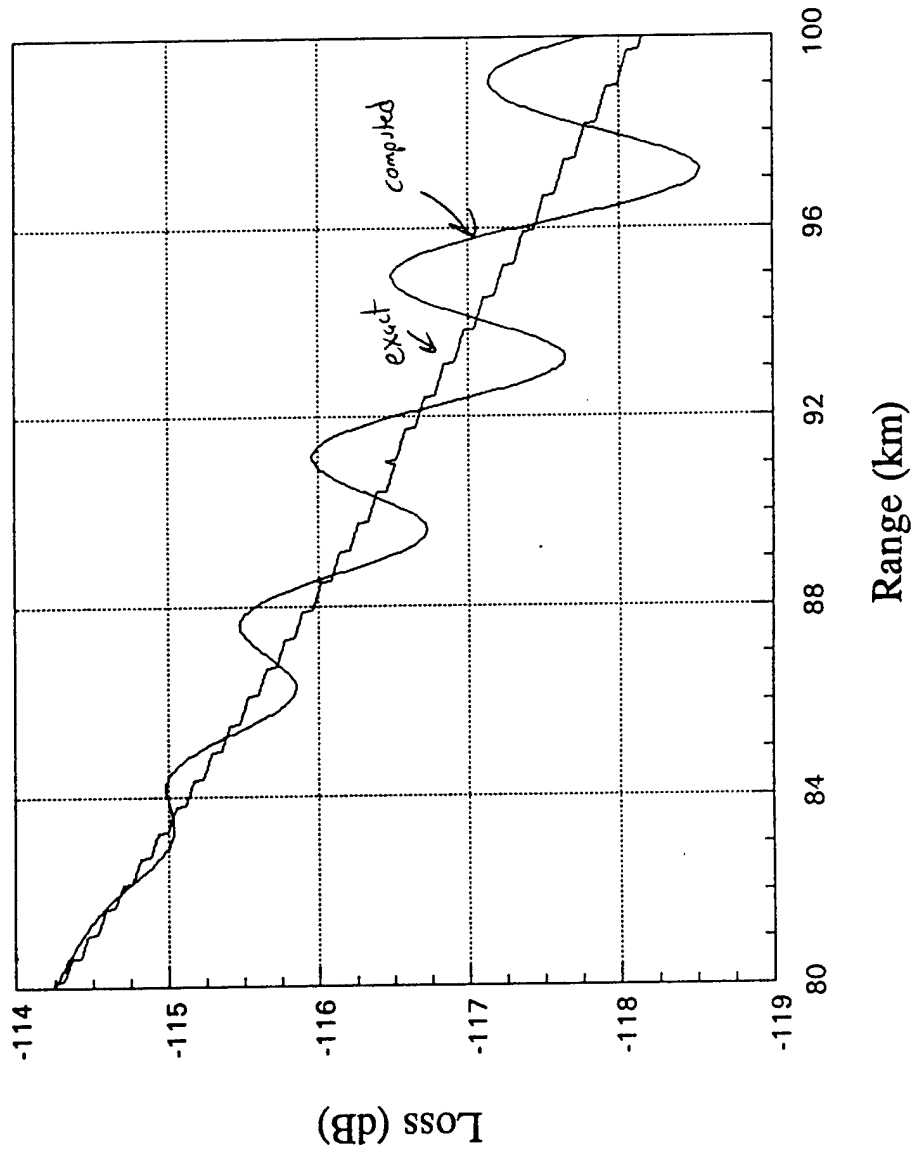
B49

# Freq. = 6.2 MHz (Interpolation Check)

HMAX $\ell$ = 5000 m

errors are $O(10^{-2.5})$ $O(10^{-1})$ dB

Not R d

Loss (dB)

-117.0

-117.3

-117.6

-117.9

-118.2

-118.5

96    97    98    98    99    100

Range (km)

(Psi)

BSO

Freq. = 72.1 MHz (Interpolation Check)

xMAXA = 2000 m

Loss (dB)

Range (km)

~12,500 λ

λ = 4.152m

(16a)

$Z_s$ = 151 m
$Z_r$ = 82 m
dr = 5

B51

Freq. = 72.1 MHz (Interpolation Check)

Hmax1 = 2000

Range (km)

Loss (dB)

(16b)

# Freq. = 72.1 MHz (Interpolation Check)
Hmax1, 2000m

## Range (km)

## Loss (dB)
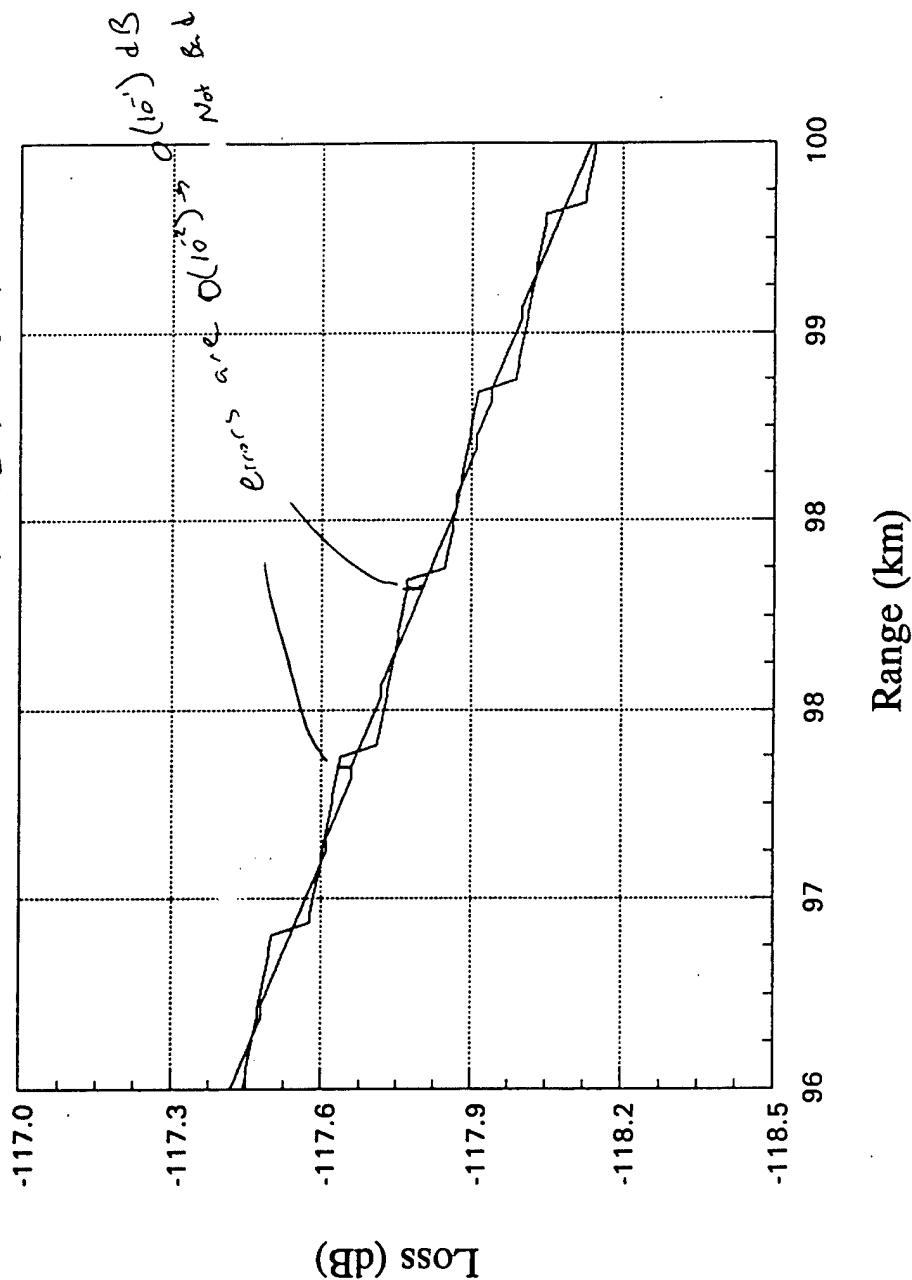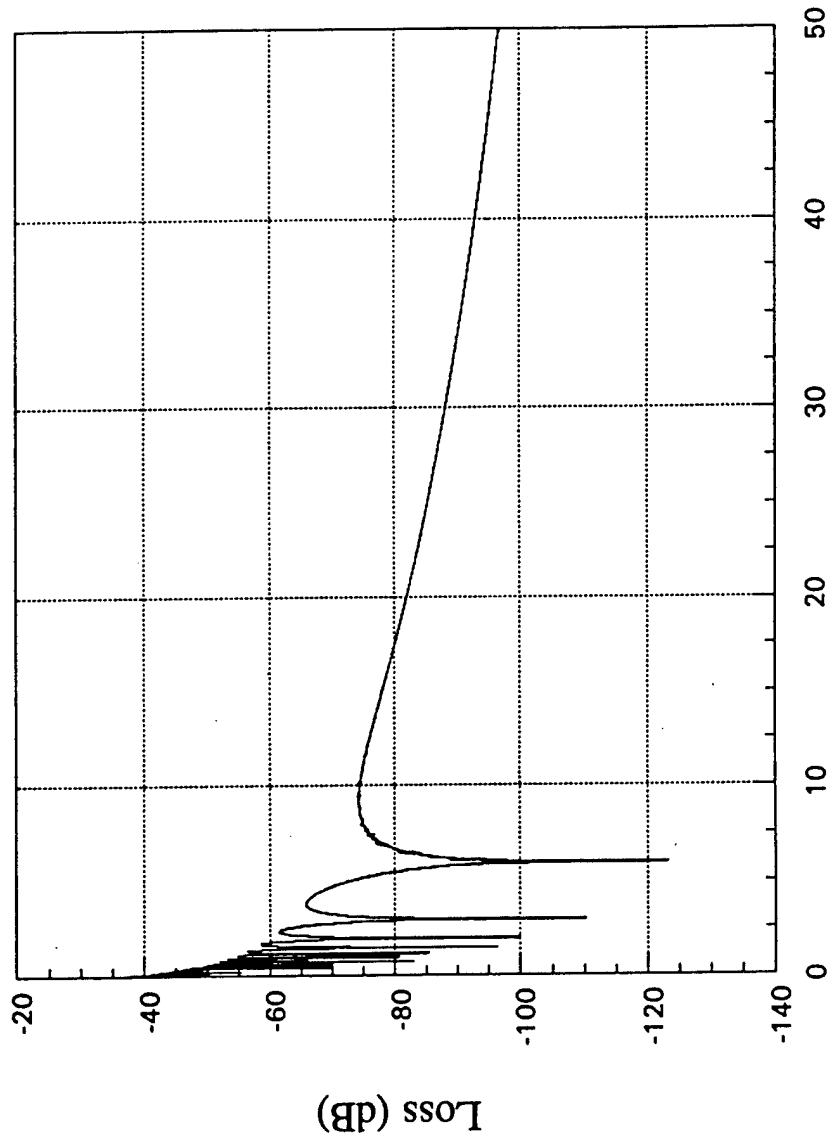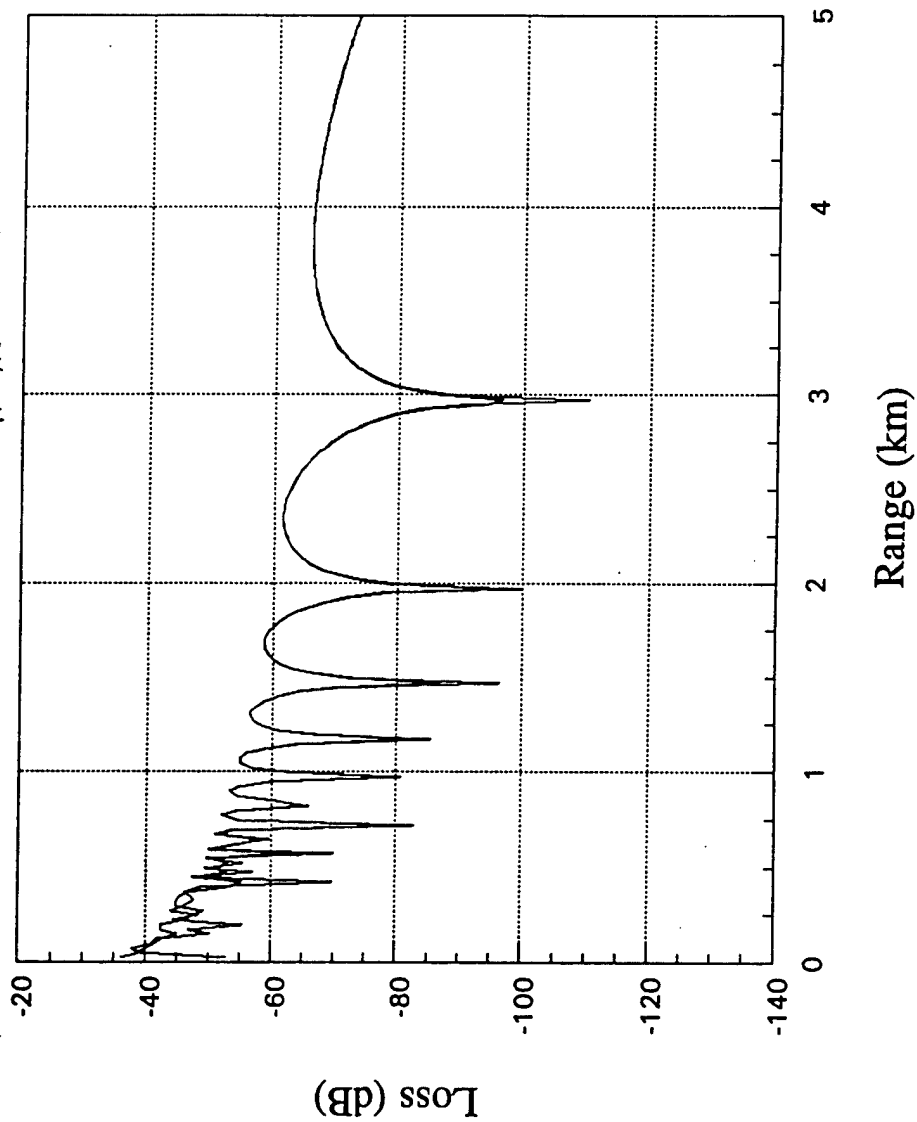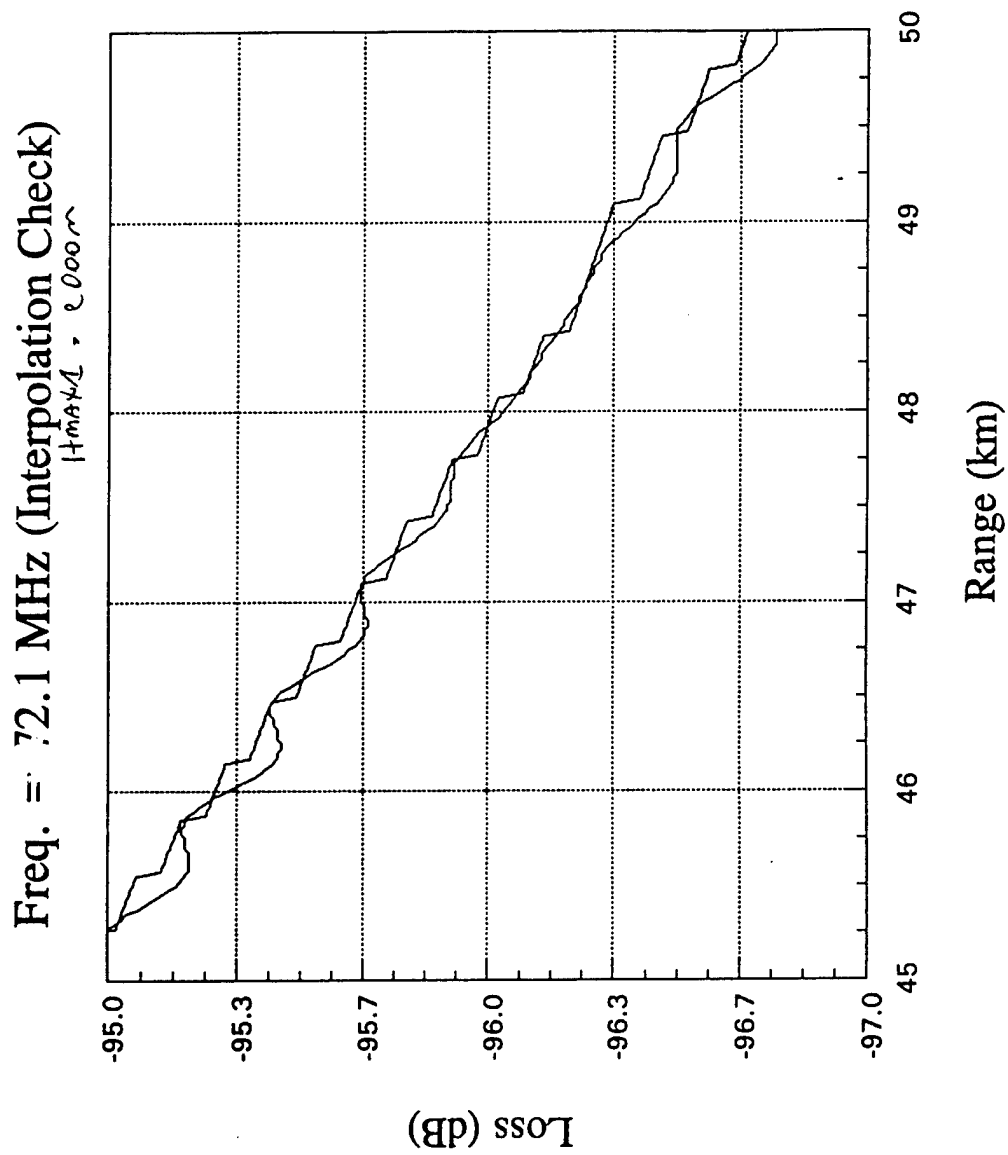
(16c)

# Appendix C
## Source Modeling Results

# SSP Source Model Sensitivity Analysis

In the process of studying the absorbing layer problem, discussed in the last section, I found that a detailed analysis of the source models used in SSP was necessary. It seemed that solutions converged only after the grid sizes smaller than three points per wavelength. Since the efforts would yield preliminary source sensitivity data this was very important. There are three types of source models used in SSP

## Gaussian Model

$$\text{real}(u) = \sqrt{\frac{k_0}{2}} \left( \exp\left( -\frac{k_0^2 (z - z_s)^2}{4} \right) - \exp\left( -\frac{k_0^2 (z + z_s)^2}{4} \right) \right)$$

## Green's Function Model

$$\text{real}(u(z)) = \sqrt{\frac{k_0}{2}} \left( \alpha(z - z_s) \exp\left( -\frac{k_0^2 (z - z_s)^2}{3.0512} \right) - \alpha(z + z_s) \exp\left( -\frac{k_0^2 (z + z_s)^2}{3.0512} \right) \right)$$

where
$$\alpha(z) = \left( 1.4467 - 0.4201 k_0^2 z^2 \right)$$

## Normal Mode Model

$$\text{real}(u(z)) = \frac{2\sqrt{2\pi}}{z_{max}} \int \frac{\sin(k_z z_s) \sin(k_z z)}{\sqrt{k_0^2 - k_z^2}} dk_z$$

While the rule of thumb in the under water acoustics community is three points per wavelength for grid sizes, this choice is seemingly too sparse for some of the source models in SSP. Figures 1-3 (found at the end of the discussion) show the real part of the solution generated by the three source models for three frequency cases of f = 5, 10 and 50 MHz. The medium is assumed to be 250 m high, and the source is at 100 m. In Figure 1(a), where the source frequency is 5 MHz, and dz is 25 m, the Gaussian startup (rep circle) is non zero at only 3 points. The Green's startup is non zero at 7 points. The normal mode is very different with its side lobes, but there still is a rough sampling of the oscillations. When decreasing dz to 10 m, as in Fig 1(b) already there is a better sampling. Figures 1(c) and 1(d) show over sampled cases. The same is true for higher frequencies as show for f = 10 MHz (Figure 2,) and f = 50 MHz (Figure 3). Since the oscillations become so wild at 50 MHz blowups are show zeroing in on the interval [75,125] km.

C1.

However, it is apparent from examine normal mode startup fields that for $f = 5$ MHz, when $dz = 10$ m ( 6 points per wavelength) the trig functions are sampled well. For $f = 10$ MHz, $dz = 5$ m gives a similar sampling as in the $f = 5$ MHz case. Finally for $f = 50$, as expected the sampling rate is the same when $dz = 1$m. As for the Green's function and Gaussian function startup fields, one can calculate the $dz$ by fixing the number of points needed for a fixed fall-off rate. That is if we let

$$z - z_s = i\, dz$$

then the main contributing exponential is at $1/e$ when the argument

$$\frac{k_0^2 dz^2 i^2}{3.0512} = 1 \text{ for Green's startup}$$

and

$$\frac{k_0^2 dz^2 i^2}{4} = 1 \text{ for Gaussian startup.}$$

So for example to sample the main beam of a Gaussian startup with 5 points, 2 on each side, set $i = 2$ and the equation gives

$$dz = \frac{1}{k_0} \ .$$

For $f = 5$ MHz, this equation gives $dz = 9.6$, for $f = 10$ MHz, this equation gives $dz = 4.8$, and for $f = 50$ MHz, this equation gives $dz = .96$. Checking the figures (1b), (2b), and (3c), we see it is true. The main lobe falls to $1/e$ of its maximum value by the second notch point on each side. And since

$$k_0 = \frac{2\pi f}{c_0} = \frac{2\pi}{\lambda}$$

this means that

$$dz = \frac{\lambda}{2\pi} \approx \frac{\lambda}{6},$$

C2

or approximately six points per wavelength. However, from my test runs I don't believe this is a fine enough mesh for proper source sampling. I suggest a minimum of 12 points per wavelength for convergent solutions (as far as the source model is concerned).

For now this can be handled by tolerating longer run times, however, for intensive computation this might be too stringent. An adaptive routine might be desirable. That is one that starts out with a mesh for proper source sampling, then after a few steps cuts back on the mesh size. This is not a trivial matter, and it has been decided to table that effort and study the real problem encountered.

As for a comparison of source models, it appears that in the far field removed from the source, it really does not matter which particular source one chooses. In Figure 4 I have plotted the losses for the three different source models. In the near field at ranges less than 10 km ( Fig 4(b) and 4(c)), the solutions do disagree. but by the far-field at ranges of 20 to 25 km (Fig 4(d)), all three solutions agree quite excellently. I thought that the absorbing layer might be influencing the results so I ran the problem again without it. These results are shown in Figure 5. By ranges of 5 km, all three solutions already agree well. (Fig 5(c) and 5(d).). In Figure 6 the frequency has been raised to 10 MHz. Similar results are seen with excellent agreement. Finally in Fig 7, frequency is raised to 25 MHz, and there is still excellent agreement between the solutions in the far-field.

F5DZ25.ST

FREQ = 5 MHz

DZ = 2.5 m
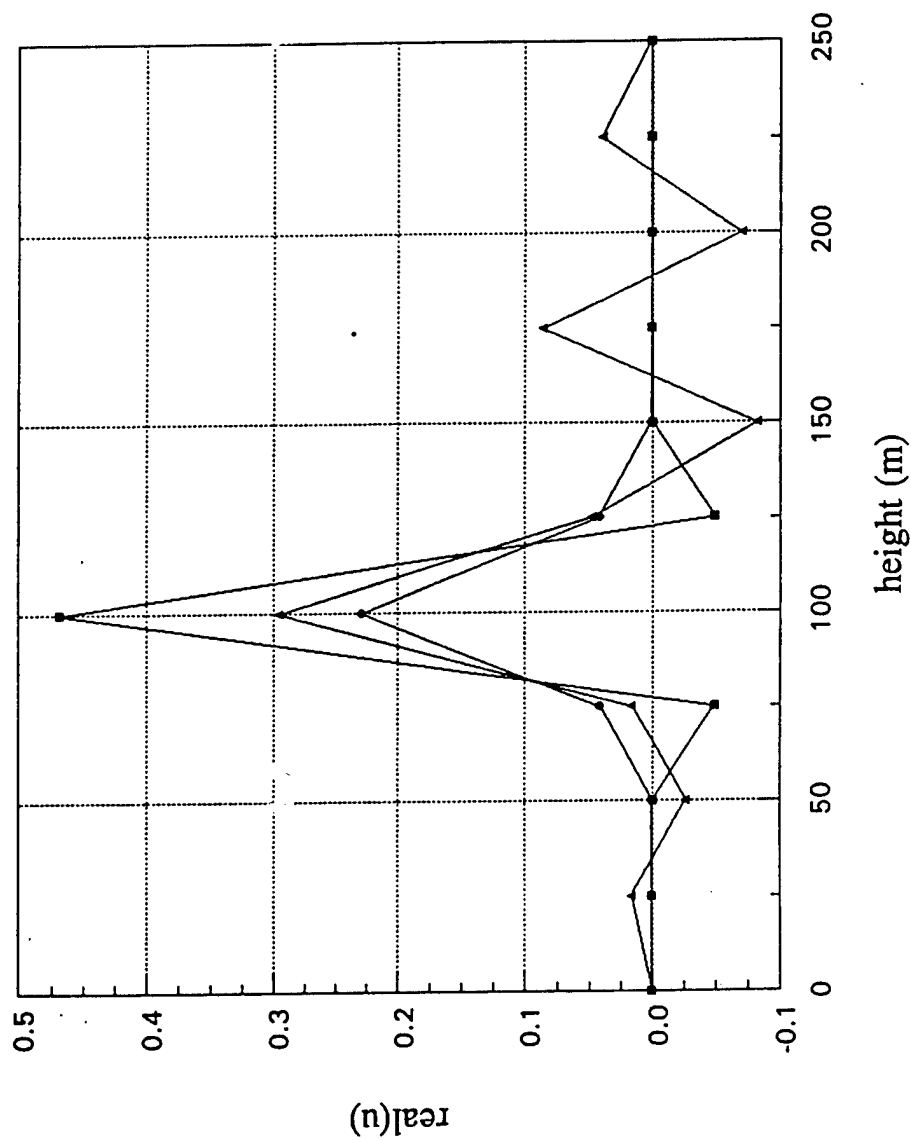
LEGEND

● GAUSSIAN START UP

■ GREEN'S FUNCTION START UP

▲ NORMAL MODE START UP VI THMAX = 8.5 (omnidirectional)

Fig 1q

C4.

F5DZ10.ST

FREQ = 5 mHz

Δz = 10

(1b)

height (m)

real(u)

CS

F5DZ5.ST

height (m)

real(u)

(1c)

C6

F5DZ1.ST

real(u)

height (m)

(h)

C7

# F10DZ10.ST



height (m)

real(u)

( 2𝒸 )

c8

F10DZ5.ST

height (m)

real(u)

( 2b )

C9

F10DZ1.ST

height (m)

real(u)

(3c)

C10

F10DZP5.ST

(2d)

F50DZ2.ST

(3a)

C12

F50DZ2.ST

height (m)

real(u)

(3ᵇ)

F50DZ1.ST

real(u)

height (m)

(3c)

C14

F50DZ.5.ST

Column1-
Heykt (m)

(3d)

Column2

Loss (dB)

C15

Source Model Comparison (f=5 MHz)

W ABSORBING LAYER

Loss (dB)

Range (km)

GAUSSIAN
GREEN'S
MODE

($^4/_5$)

C16

# Source Model Comparison (f=5 MHz)

3  ABSORBING  LAYER

Range (km)

Loss (dB)

(4h)

C17

Source Model Comparison (f=5 MHz)

ω Absesing Layer

Range (km)

Loss (dB)

(4c)

C18

# Source Model Comparison (f=5 MHz)



Range (km)

Loss (dB)

(h)

C19

# Source Model Comparison (f=5 MHz)

w/o Absorbing Layer

Loss (dB)

Range (km)

(5q)

Source Model Comparison (f=5 MHz)

C/o Absorbing Layer

Range (km)

(5b)

Loss (dB)

Source Model Comparison (f=5 MHz)

w/o Assessing later

Range (km)

Loss (dB)

(5c)

C22

Source Model Comparison (f=5 MHz)

w/o Absorbing Later

Range (km)

(5d)

Loss (dB)

# Source Model Comparison (f=10 MHz)

*w/o A L.*



Loss (dB)

Range (km)

( 6 )

Source Model Comparison (f=10 MHz)

w/o n l,

Loss (dB)

Range (km)

(6b)

**Source Model Comparison (f=10 MHz)**

we at.

Range (km)

Loss (dB)

(6c)

C26

Source Model Comparison (f=10 MHz)

W/o A.L.

Loss (dB)

Range (km)

(b)

C27

Source Model Comparison (f=25 MHz)

w/c A.L.

Loss (dB)

Range (km)

(7')

C28

# Source Model Comparison (f=25 MHz)

w/o A.L.



Range (km)

(7b)

Loss (dB)

C29

# Source Model Comparison (f=25 MHz)

w/o A.L.



Loss (dB)

Range (km)

(2c)

C30

# Source Model Comparison (f=25 MHz)

w/o A L.

Loss (dB)

Range (km)

(7d)

C31